Neurosci. Bull. September, 2023, 39(9):1375–1395
https://doi.org/10.1007/s12264-023-01042-9

www.neurosci.cn
www.springer.com/12264

ORIGINAL ARTICLE

The Circadian System Is Essential for the Crosstalk of VEGF-Notch-mediated Endothelial Angiogenesis in Ischemic Stroke

Yuxing Zhang[1,2,3] · Xin Zhao[3] · Chun Guo[1] · Ying Zhang[1,3] · Fukang Zeng[1,2,3] · Qian Yin[3] · Zhong Li[1] · Le Shao[3,4] · Desheng Zhou[1] · Lijuan Liu[1]

Received: 28 October 2022 / Accepted: 18 December 2022 / Published online: 2 March 2023

Abstract Ischemic stroke is a major public health problem worldwide. Although the circadian clock is involved in the process of ischemic stroke, the exact mechanism of the circadian clock in regulating angiogenesis after cerebral infarction remains unclear. In the present study, we determined that environmental circadian disruption (ECD) increased the stroke severity and impaired angiogenesis in the rat middle cerebral artery occlusion model, by measuring the infarct volume, neurological tests, and angiogenesis-related protein. We further report that Bmal1 plays an irreplaceable role in angiogenesis. Overexpression of Bmal1 promoted tube-forming, migration, and wound healing, and upregulated the vascular endothelial growth factor (VEGF) and Notch pathway protein levels. This promoting effect was reversed by the Notch pathway inhibitor DAPT, according to the results of angiogenesis capacity and VEGF pathway protein level. In conclusion, our study reveals the intervention of ECD in angiogenesis in ischemic stroke and further identifies the exact mechanism by which Bmal1 regulates angiogenesis through the VEGF-Notch1 pathway.

✉ Desheng Zhou
zds1101@foxmail.com

✉ Lijuan Liu
601264967@qq.com

[1] Department of Neurology, The First Hospital of Hunan University of Chinese Medicine, Changsha 410007, China

[2] Key Laboratory of Hunan Province for Integrated Traditional Chinese and Western Medicine on Prevention and Treatment of Cardio-Cerebral Diseases, Changsha 410208, China

[3] Hunan University of Chinese Medicine, Changsha 410006, China

[4] Laboratory of Prevention and Transformation of Major Diseases in Internal Medicine of Traditional Chinese Medicine, Changsha 410007, China

Keywords Circadian clock · Ischemic stroke · Angiogenesis · VEGF · Notch pathway

Introduction

Ischemic stroke (IS) is the second leading cause of death worldwide: >15 million people suffer a stroke each year, and ~5 million more are permanently disabled [1–3]. IS is characterized by high morbidity, disability, mortality, recurrence, and economic burden [4]. At present, the treatment of IS mainly relies on reperfusion therapy, including thrombolysis and thrombectomy. Thrombolysis mainly uses recombinant tissue plasminogen activator (rt-PA), which is currently the only therapeutic drug approved by the US Food and Drug Administration, while thrombectomy is mainly endovascular treatment, i.e., mechanical thrombectomy [5, 6]. However, because of the very limited time window and the risk of hemorrhagic events, rt-PA can only be used in <10% of patients with stroke, and the success rate of re-canalization is <50% [7, 8]. In this context, the research on neuroprotective agents is extensive, but it is regrettable that so far there have been no exciting translation results from medical research to clinical practice [9].

Previous studies have reported that repair of the damaged neurovascular unit (NVU), especially angiogenesis, contributes to the establishment of collateral circulation and plays a pivotal role in the recovery from ischemic stroke injury [10, 11]. Angiogenesis is a complex process in which a large number of substances are released to participate in angiogenesis after an ischemic stroke. Hypoxia-induced angiogenesis, which occurs in the ischemic penumbra within hours of stroke and persists for several weeks [12], is one of the major events in an adaptation to glucose deficiency and hypoxia, and is critical

for maintaining cell metabolism, survival, and function [13, 14]. After a stroke, ischemic penumbra tissue releases angiogenesis factors, including vascular endothelial growth factor (VEGF), matrix metallopeptidases (MMPs), platelet-derived growth factor, and angiogenin (Ang), which promote basement membrane degeneration, extracellular matrix (ECM) remodeling, and endothelial cell (EC) proliferation and migration, resulting in the formation of neovascularization, thereby improving collateral circulation [15, 16]. Clinical studies have confirmed that patients with high cerebrovascular density have better functional recovery and longer survival times than those with low cerebrovascular density [17–19]. Therefore, promoting angiogenesis in patients has gradually become a promising strategy for the treatment of ischemic stroke.

Circadian rhythms are endogenous oscillations at the cellular level, with a period of ~24 h, that regulate cellular metabolism and behavioral output [20, 21]. Circadian rhythms determine cell fate, including neurons, glia, ECs, neutrophils, and macrophages, which are involved in angiogenesis and the immune response process in ischemic stroke [22, 23]. Briefly, the core circadian proteins Bmal1 and Clock act as transcriptional factors that bind to form a heterodimer and then enter the nucleus to bind the E-box regulatory elements of the Period (Per1, Per2, Per3) and Cryptochrome (Cry1, Cry2) genes, activating their transcription. However, Per and Cry family proteins accumulate in the cytoplasm, and together with casein kinase 1δ (CK1δ) and CK1ε, they translocate to the nucleus and inhibit the transcription of Clock and Bmal1 [24, 25]. In addition to targeting the Per and Cry genes, the Clock: Bmal1 heterodimer activates the transcription of Rev-erbα and Rev-erbβ, which compete at Rev-erb/retinoic acid-related orphan receptor (ROR) binding elements with RORα, RORβ, and RORγ [26, 27]. The third transcriptional loop activated by the Clock: Bmal1 heterodimer involves the PAR-bZip (proline and acidic amino acid-rich basic leucine zipper) factors, including DBP (D-box binding protein), TEF (thyrotroph embryonic factor), and HLF (hepatic leukemia factor). These proteins interact at D-box-containing sites with the Rev-erb/ROR loop-driven repressor NFIL3 (nuclear factor, interleukin 3 regulated; or E4BP4) [28–30]. Recent studies have shown that the circadian rhythm significantly affects the susceptibility, injury, recovery, and treatment response mechanisms of stroke [31]. Shift work-induced environmental circadian disruption (ECD) increases stroke severity and immune response dysregulation [32[. As for angiogenesis, studies have confirmed that the circadian rhythm transcription factor Bmal1 (aryl hydrocarbon receptor nuclear translocator-like 1) has a positive regulatory effect on the increase of VEGF-A, a key molecule induced by hypoxia-induced angiogenesis, but a negative regulatory effect has been reported in Per2 and Cry1 [33, 34], and further research has demonstrated that Bmal1 directly binds to the promoter region of VEGF and regulates the promoter activity [35].

Several studies have shown that the Notch signaling pathway interacts with VEGF under hypoxic conditions to jointly regulate arterial properties and angiogenesis [36]. Preliminary research on VEGF and Notch pathways comes from the study of vasculogenesis. The results suggest that VEGF plays a role in angiogenesis by regulating the expression of Notch1 and Dll4 upstream of the Notch pathway [37, 38]. Furthermore, in stroke models, the Notch signaling pathway is involved in the formation of collateral networks in ischemic stroke. Inhibition of Notch signaling affects tissue perfusion by restricting arterial structure and function, impairing the repair of angiogenesis after ischemia [39, 40].

In the present study, we aimed to investigate the effect of circadian rhythms on hypoxia-induced collateral vessel formation after ischemic stroke and the potential pro-angiogenic mechanism of the core circadian genes. Therefore, we constructed a rat middle cerebral artery occlusion (MCAO) and environmental circadian disruption (ECD) model, and a mouse brain microvascular EC (bEnd.3) oxygen-glucose deprivation/re-oxygenation (OGD/R) model. We further determined the relationship between ECD and angiogenesis after ischemic stroke and the role of Bmal1 on the angiogenic process after OGD/R intervention. These results suggested that ECD significantly increased the severity of the ischemic stroke, impaired the ability of angiogenesis, and reduced neurological recovery. The core clock gene Bmal1 was also confirmed to be a potential therapeutic target to promote angiogenesis after ischemia-hypoxic injury by regulating the expression of VEGF and Notch signaling pathways.

Materials and Methods

Ethics Statement

All animal experiments were performed in accordance with the guidelines of the China Council on Animal Care and Use. This study was approved by the Laboratory Animal Professional Committee of the First Affiliated Hospital of Hunan University of Chinese Medicine (Approval no. 20201010-13). Every effort was made to minimize pain and discomfort to the animals. Animal experiments were performed in The First Affiliated Hospital of the Hunan University of Chinese Medicine. All rats were kept in cages with suitable temperature (23°C–25℃) and humidity (40%–60%) and were randomly divided into 3 groups. The rats had unrestricted access to food and water.

Circadian Disruption Protocol

Sprague-Dawley rats were used in this experiment. Before the intervention, rats were housed for 2 weeks to acclimate to the housing facilities and handling. The rats were then randomly assigned to various experimental groups, and they were kept in cages for the rest of the study. Rats were assigned to a standard 12:12 LD schedule ($n = 40$) or a chronic LD shift schedule ($n = 20$) for a 44-day light intervention (Fig. 1A). This lighting schedule causes ECD, which has been reported in many articles [32, 41, 42]. In this timetable, by advancing the dark cycle, the 12:12 LD cycle was advanced by 6 h, once every 7 days. Rats were given standard rat food after arriving at the facility. Rat food and water were freely available.

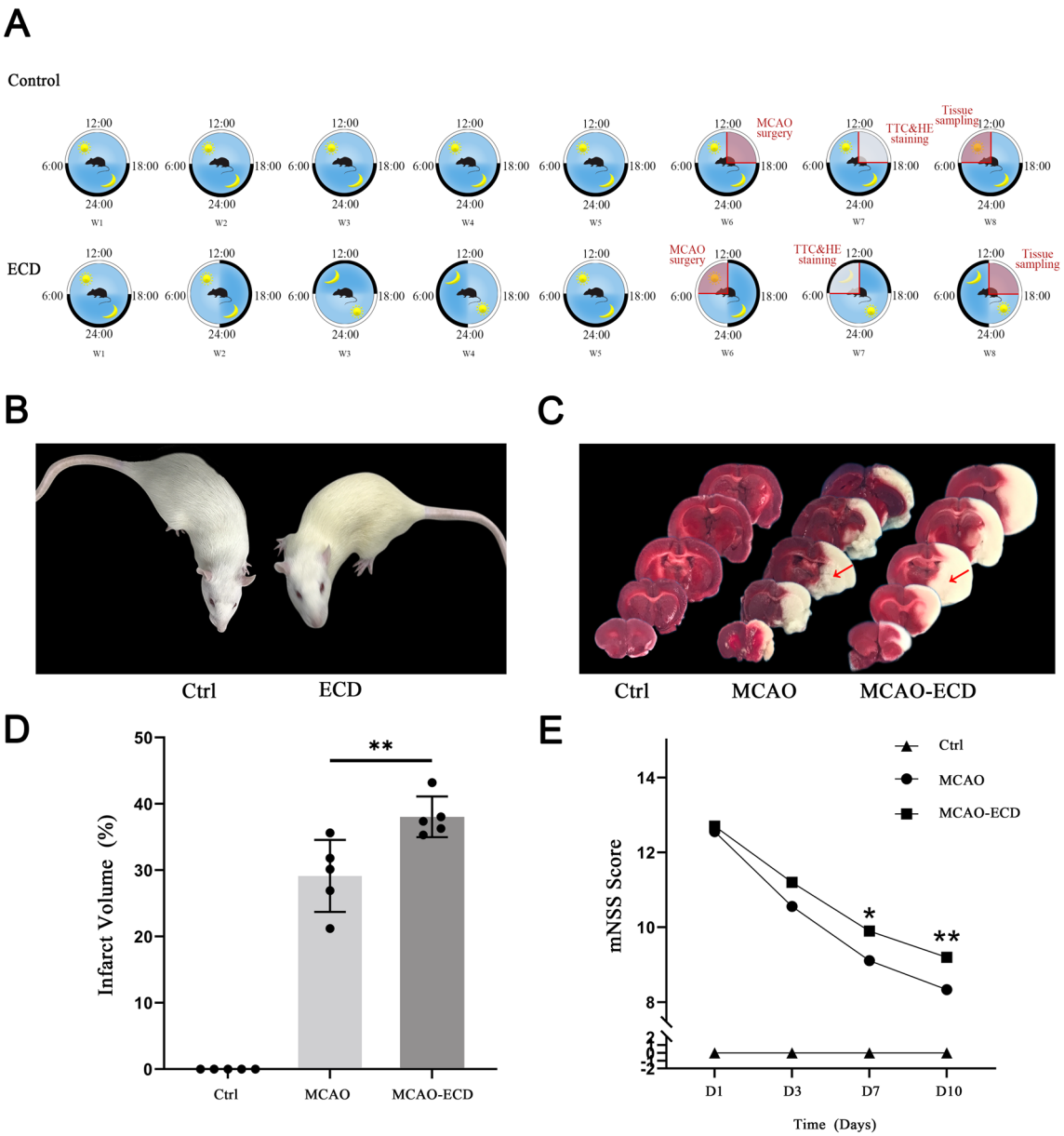

Fig. 1 Environmental circadian disruption increases stroke severity. **A** ECD protocol. Rats were assigned to stay on the standard 12:12 LD schedule or exposed to the shortening of the dark period: the 12:12 LD cycle was advanced by 6 h once every 7 days for 44 days. The red ranges show the times of surgery and sampling. **B** Representative images of the dorsal hair of mice; left, a non-ECD rat (Ctrl); right, an ECD rat. **C**, **D** Representative images and bar graphs showing the brain lesions in Ctrl, MCAO, and MCAO-ECD rats, 24 h after MCAO surgery ($n = 5$) The red arrow indicates the infarct area. **E** Bar graphs summarizing the results of mNSS score in Ctrl, MCAO, and MCAO-ECD rats ($n \geq 10$). Data are presented as the mean ± SD. $^*P < 0.05$, $^{**}P < 0.01$.

The Middle Cerebral Artery Occlusion and Reperfusion (MCAO/ R) Model

The MCAO procedure was scheduled on the last day of week 6 of the ECD protocol. Considering the difference in illumination time, the MCAO operation in the ECD group was performed at 06:00–12:00, and in the control group it was performed at 12:00–18:00. The rats fasted for 12 h before the operation, but they were still free to drink water during this period. The anesthetized rats were placed in a supine position on a scaffold, under sterile conditions, the right common carotid artery, external carotid artery, internal carotid artery (ICA), and the junction of the carotid artery were carefully exposed through a midline neck incision. A silicon-coated suture (head diameter 0.36 ± 0.02 mm, Beijing Senbi Biotechnology Co., Ltd., Beijing, China) was inserted into the external cervical incision, and the blood flows through the ICA to the beginning of the middle cerebral artery was blocked for 2 h; reperfusion was simulated by removing the suture. The temperature was maintained at 37 ± 0.5°C with a thermostatic surgical pad. After the operation, all rats were placed on a warm blanket until recovery.

Neurological Tests

Modified neurological severity scores (mNSS) were evaluated by a blinded observer using an 18-point scoring system 24 h after reperfusion and completed within the first 2 h after illumination was initiated on each of the subsequent 3, 7, and 10 days. Scores were assigned according to the following six tests: spontaneous activity, limb symmetry, forepaw outstretching, climbing, body proprioception, and response to vibrissal touch. Each score was the total of scores for each of the six tests (minimum score, 3; maximum score, 18).

Triphenyl-Tetrazolium Chloride (TTC) Staining

TTC staining was applied 24 h after the operation in each group. Brains from 5 rats in each group were frozen at –20°C for 20 min. Then each brain was cut into 2-mm-thick coronal slices and immediately stained with phosphate-buffered saline (PBS; Procell, Wuhan, China) containing 2% TTC (Sigma, Saint Louis, MO, USA) in a 37 ℃ incubator for 30 min, fixed with 4% paraformaldehyde, and photographed. The infarct areas appeared white while the normal areas were red. The cerebral infarction ratio was measured by Image-Pro Plus software (i.e., the percentage of the area of the infarct area to that of the ipsilateral cerebral hemisphere).

Cerebral Histopathology (HE Staining)

After 24 h of reperfusion in each group, rat brain samples were collected into cryovials containing 4% paraformaldehyde. The samples were dehydrated and embedded in paraffin, and coronal sections were cut. These sections were then stained with hematoxylin and eosin (HE) and used for histopathology. Finally, images were acquired by light microscopy (Leica, Wetzlar, Germany) to assess histopathological changes in the hippocampus.

CD34 Immunofluorescence Staining of Rat Hippocampus and Cortex

The presence of CD34 in the hippocampus and cortex of each group was detected by immunofluorescence 10 days after reperfusion. To minimize the factor of the endogenous circadian phase, the timing of brain sampling in control and MCAO groups was conducted during 06:00–12:00, while that in the MCAO-ECD group was from 12:00 to 18:00. Coronal sections were collected and prepared as described above. Before staining, the sections were deparaffinized and rehydrated, and antigen retrieval was applied. Afterward, the sections were blocked with 5% BSA for 1 h at room temperature. Then, the sections were incubated at 4℃ overnight with anti-CD34 (ab81289, Abcam,1:200). Next day, the sections were washed 3 times with PBS and incubated with CoraLite594 (SA00013-4, Proteintech, 1:400) for 2 h at room temperature. After rinsing, the nuclei were stained with DAPI for 15 min. The number of immunoreactive cells in predefined areas was quantified using ImageJ software (NIH, Bethesda, MD, USA). Cells were counted by blinded observers in three different fields of view for each mouse in each group of three mice.

ELISA of Melatonin, VEGF, IL-1β, IL-18, and TNF-α

The timing of serum sampling in each group was the same as described above. Blood samples were taken from the abdominal aorta in ethylenediaminetetraacetic acid (EDTA)-containing tubes and the plasma was separated. The concentrations of melatonin, VEGF, IL-1β, IL-18, and TNF-α in plasma samples from both groups were measured by ELISA Complete Kits (Cusabio Biotech, Wuhan, China) according to the manufacturer's protocol using an Elisa reader to record optical density. The final concentrations of melatonin were calculated based on a standard curve constructed using hormone standards. Each sample was evaluated in triplicate and the mean concentration was used for further analysis.

Cell Circadian Gene Induction and OGD/R Treatment

bEnd.3 cells (mouse brain microvascular ECs) were used for further phenotyping and molecular biological assessment of angiogenesis [43, 44], and were donated by Dr. Yan Shang and Lumei Liu, for which we are very grateful. bEnd.3 cells were cultured in Dulbecco's modified Eagle's medium

(DMEM; Procell, Wuhan, China) supplemented with 10% fetal bovine serum (Procell, Wuhan, China), 1% penicillin, and streptomycin, and placed in an incubator with 5% CO_2 at 37°C. bEnd.3 cells were sub-cultured when the cell density reached 90%. Finally, the cells used for the subsequent experiments were in the logarithmic growth phase.

To synchronize the rhythmic circadian gene expression, bEnd.3 cells were cultured in complete medium containing dexamethasone (100 nmol/L) for 2 h [9, 45]. Then cells were harvested or subjected to OGD at the indicated time points. Before OGD exposure, the culture medium was replaced with glucose-free DMEM and the cells were incubated for 6 h at 37°C in an atmosphere of 5% CO_2 and 95% N_2. Afterward, the glucose-free medium was replaced with the complete medium, and the cells were returned to the incubator (with O_2) for 24 h.

DAPT Treatment

To verify the proportion of the Notch1 signaling pathway *in vitro* study, we used DAPT (HY-13027, MCE, Princeton, NJ), a gamma-secretase inhibitor. DAPT inhibits the formation of soluble Notch intracellular domain (NICD) proteins by preventing γ-secretase cleavage at the S3 site of the Notch receptor, preventing NICD translocation to the nucleus. DAPT was diluted in dimethyl sulfoxide to 10 mmol/L mother liquor, and cells were maintained in a complete medium containing 10 μmol/L DAPT when cultured. Before OGD, bEnd.3 cells were incubated in a serum-free medium in the presence or absence of 10 μmol/L DAPT for 24 h [46–48]. The DAPT intervention was continued during and after the OGD process until the end of each experiment, including scratch wound assays, migration assays, and tube formation assays.

Lentivirus Vector Infection for Bmal1 Overexpression and Knockdown

The overexpression lentivirus vector was constructed by Genechem Co., Ltd. (Shanghai, China). The sequence used for PCR amplification of mouse Bmal1 is shown below: Arntl-21735-P1: AGGTCGACTCTAGAGGATCCCGCCACCATGGCGGACCAGAGAATGGACATTTC; Arntl-21735-1-P2: TCCTTGTAGTCCATACCCAGCGGCCATGGCAAGTCACTAAAG. Double-stranded oligonucleotides were inserted between the Ubi-MCS-3FLAG-CBh-gcGFP-IRES-PUR plasmid BamHI/AgeI restriction sites, and the linked plasmids were transformed into *Escherichia coli* DH-5α competent cells for plasmid amplification. And the mouse Bmal1 siRNA Lentivirus vector construction and packaging services were provided by Hanbio Co., Ltd. (Shanghai, China). The interference target design and primers were as follows: siRNA1: GCTTGTTTGACTACCTGCATCCAAA; siRNA2: CGGGTGAAATCTATGGAGTACGTTT; siRNA3: CAGTAACGATGAGGCAGCAATGGCT. Double-stranded oligonucleotides were inserted between the pHBLV-U6-MCS-CMV-ZsGreen-PGK-PURO plasmid BamHI/EcoRI restriction sites, and the linked plasmids were transformed into *E. coli* DH-5α competent cells for plasmid amplification. Plasmids from positive colonies were verified by RT-PCR and DNA sequencing.

bEnd.3 cells were prepared as suspensions and inoculated into a 6-well plate at 5–8 × 10^4 cells per well and incubated for 24–36 h. Once they reached 35%–50% density, a suitable volume of the lentivirus infection reagent was added to the culture medium based on an MOI of 30. After 24 h, the medium was replaced with a complete medium. At 72 h after transfection, the transfection efficiency was determined by the expression of green fluorescent protein (GFP). Then, the bEnd.3 cells were sub-cultured in a medium containing 6 μg/mL puromycin for further selection. A single transduced stable cell line was established and used for all subsequent cell cultures and each experiment after transduction.

Chromatin Immunoprecipitation Sequencing (ChIP-seq)

Approximately 3 × 10^7 bEnd.3 cells were cross-linked with 1% formaldehyde for 20 min when the confluence reached 90%. The cross-linking reaction was quenched by adding glycine to a final concentration of 125 μmol/L. After washing three times with cold PBS, nucleus lysate was collected by centrifugation and re-suspended in 300 μL of nuclear lysis buffer (50 mmol/L Tris-HCl pH 8.0, 1% SDS, 10 mmol/L EDTA). After centrifugation at 17,000 r/min for 15 min at 4°C, the fragmented chromatin was diluted 1:5 with IP dilution buffer (20 mmol/L Tris-HCl pH 8.0, 150 mmol/L NaCl, 1% Triton X-100, 1 mmol/L EDTA) supplemented with 1× protease inhibitor cocktail, and incubated with 10 μg anti-Bmal1 (ab230822, Abcam) overnight at 4°C. 100 μL of Dyna bead Protein A (Invitrogen 10002D) was added and the mixture was incubated for another 3 h. After washing three times, 200 μL of direct elution buffer was applied to the bead pellet along with RNAse A and reverse cross-linked at 65°C overnight. Then proteinase K was applied and incubated at 55°C for 2 h. Finally, DNA was purified by the following deep sequencing (ChIP-seq) (SeqHealth Tech, China). For ChIP-seq results, after obtaining raw sequencing data (raw data), they were filtered and high-quality sequencing data (clean data) were subjected to further comparative analysis. The results were then compared with genome-wide *de novo* peak calling to investigate the binding preferences of proteins across the genome, and motif analysis of binding sites was applied.

High-throughput sequencing using Illumina sequencers requires the construction of a matching sequencing library.

FASTP (version 0.23.0, Shifu Chen 2018 GeneFuse: detection and visualization of target gene fusions from DNA sequencing data) was used for the quality control and filtering of raw reads. The sequencing results were compared with the mouse reference genome (Mus_musculus. GRCm38) *via* bowtie1 (v 2.1.0). The Picard tool was used to select the non-duplicate uniquely mapped reads on the reference genome for subsequent analysis (http://picard.sourceforge.net). MACS14 was used to search the peak value of the ChIPseq, and input DNA was used as the control [49]. A significant threshold of 10–5 was applied to all data sets. The R-package ChIP seeker [50] was used to calculate a series of statistics including relevant gene retrieval and genome element distribution analysis. Therefore, we used homer (http://homer.ucsd.edu/homer/) to extract the sequence of the interval where the peak was located, scanned the common motif among the peaks, searched the common motif region, and drew the motif map. Peak-related genes were selected for downstream Gene Ontology (GO) and Kyoto Encyclopedia of Genes and Genomes (KEGG) pathway analysis. A GO term with $q \leq 0.05$ was defined as significant enrichment after multiple test correction

Dual-Luciferase Reporter Assay

To study the potential regulatory mechanism by which Bmal1 performs its biological function in ECs, a dual-luciferase reporter assay was applied. Wild-type Notch1 promotor (PGL3-Basic-H-Notch1-WT) plasmid and Mutant-type Notch1 Promotor (PGL3-Basic-H-Notch1-MT) were constructed by the PGL3-Basic-Vector the overexpression Bmal1 plasmid (GTP-H-Bmal1) was constructed by the GTP Vector. Then, 293T cells were co-transfected with PGL3-Basic-H-Notch1-WT, PGL3-Basic-H-Notch1-MT, and NC vector or GTP-H-Bmal1 and cultured for 48 h. Finally, the luciferase activity of cells was measured, with the fluorescence value of *Renilla* plasmids as the internal reference (Promega, Madison, WI, USA).

Cell Viability Assay by Cell Counting Kit-8 (CCK-8)

Cell proliferation was assessed by the CCK-8 assay according to the manufacturer's protocol (Cell Counting Kit-8, Apply Gen, China). bEnd.3 cells were inoculated onto 96-well plates at 10^4/100 μL per well and incubated at 37°C. Each group had 5 replicates and grew for 24, 48, 72, and 96 h. 10 μL of CCK-8 solution was added to each well, and the mixture was continuously incubated at 37°C for 2 h. Finally, the OD_{450} was measured by a microplate reader (Bio-Tek Instruments, USA). The proliferation curve was drawn with the time and the corresponding OD_{450} values.

Immunofluorescence Assays of Bmal1, VEGF, and Notch1 in bEnd.3 Cells

bEnd.3 cells were seeded on slides in 24-well plates and modeled with 6 h-OGD intervention. Twenty-four hours after 6h-OGD treatment, each sample was fixed in 4% paraformaldehyde for 25 min, washed three times with TBST, and then subjected to blocking with Immunol staining blocking buffer. The anti-Bmal1 (ab3350, Abcam, 1:500), anti-VEGF (ab52917, Abcam, 1:500), and anti-Notch1 (10062-2-AP, Proteintech, 1:400) antibodies were incubated separately overnight at 4°C, followed by Dylight 549 goat anti-rabbit IgG H+L (A23320, Abbkine, 1:500) and donkey anti-rabbit IgG H&L (ab150075, Abcam, 1:500) for 1 h in a dark environment at room temperature. Finally, the slides were incubated with DAPI and an anti-fluorescence quencher. The slides were analyzed using a fluorescence microscope (BX51TRF, Olympus, Japan). Three fields were randomly chosen in every sample, and the fluorescence intensity was analyzed using ImageJ software (NIH, Bethesda, MD, USA).

Scratch Wound Assay

bEnd.3 cells were plated in a 6-well plate (2×10^5 cells/well), and incubated to reach confluence. When the bEnd.3 cell density reached ~85%, they were incubated in serum-free medium for cycle synchronization, then the monolayer was scratched using a pipette tip and washed with PBS to remove the detached cells. Then the OGD treatment cells were cultured in glucose-free DMEM in an atmosphere of 5% CO_2 and 95% N_2 at 37°C for 6 h. After OGD exposure, all groups were cultured in a complete medium for 24 h, and the wound healing area was measured under a microscope at 0 h and 24 h. The group with DAPT intervention was used at the beginning of cycle synchronization and continued until the end of the experiment. The cell migration area was measured with ImageJ software, and the area was normalized to that of control cells. The closure area of the wound was calculated as follows: migration area (%) = $(A_{0h} - A_{24h})/A_{0h} \times 100\%$, where A_{0h} is the area of the initial wound area, and A_{24h} is the remaining area of the wound 24 h after the measurement point. Data were analyzed using ImageJ software (NIH, Bethesda, MD, USA).

Tube Formation Assay

The cycle synchronization process is described above. Fifty μL Matrigel Matrix (BD Biosciences, San Diego, CA) were added to the bottom of the 96-well plate and incubated at 37°C for 30 min. A total of 2×10^4 bEnd.3 cells were suspended in glucose-free medium or complete medium and seeded on polymerized Matrigel in 96-well plates. After incubation at 37°C under OGD for 6 h, tube formation was

photographed, and the images were analyzed with ImageJ. Each experiment was repeated in three replicates. Since the initial experimental modeling time was 6 h, and the optimal tube formation timing was 6 h to 9 h, 6 h was selected as the observation time point. Therefore, DAPT in the DAPT intervention group was used at the beginning of cycle synchronization and during the OGD process. The total branch length was quantified in this experiment. The total branch length is the sum of the length of branches and segments.

Migration Assay

Transwell migration assays were used to evaluate the migration of bEnd.3 cells. The cycle synchronization process is described above. A total of 2×10^4 bEnd.3 cells were seeded into the upper chamber (3422, Corning Inc., USA), and the bottom of the upper chamber was a polycarbon membrane covered with pores 8 μm in diameter. Both the upper and lower chambers were filled with glucose-free DMEM. After maintaining OGD for 6 h, the medium in the lower chamber was replaced with the complete medium as a chemoattractant. After incubation with 5% CO_2 and 95% O_2 at 37°C for 24 h, the cells remaining on the upper surface of the membrane were removed. The bEnd.3 cells on the lower surface of the membrane were fixed in 4% formaldehyde and stained with 0.1% crystal violet. The DAPT group received DAPT in both upper and lower chambers during cycle synchronization, during the OGD process, and for 24 h after OGD. The stained cells were photographed and quantified by counting five random microscopic fields using ImageJ.

Real-time Quantitative Polymerase Chain Reaction (RT-qPCR)

Total RNA was isolated from each group with the UltraPure Total RNA Extraction Kit (SimGen, Hangzhou, China). Reverse transcription was carried out with a reverse transcription kit (Novoprotein, Shanghai, China). RT-qPCR was performed with CFX96Touch (Bio-Rad, CA, USA) according to the manufacturer's protocol. The mRNA level of each target gene was normalized to β-actin. The primers used are listed in Table 1.

Western Blotting

Proteins from brain ischemic penumbra tissue and bEnd.3 cells were extracted according to the instructions of the Enhanced Ripa cracking liquid (ApplyGEN, Beijing, China),

Table 1 Primer sequences for RT-qPCR.

Gene	Sequence	Accession number
Bmal1	F: 5'-AACCTTCCCGCAGCTAACAG-3'	NM_001374642.1
	R:5'-AGTCCTCTTTGGGCCACCTT-3'	
VEGF	F: 5'-CCAGCAGAAAGAGGAAAGAGGTAG-3'	NM_001110267.1
	R: 5'-CCCCAAAAGCAGGTCACTCAC-3'	
VEGFR2	F: 5'-CTACAGACCCGGCCAAACAA-3'	NM_001363216.1
	R: 5'-CAGCTTGGATGACCAGCGTA-3'	
ANG	F: 5'-GCAGAAGCAACAACTGGAGC-3'	NM_001286062.1
	R: 5'-TCCTCCCTTTAGCAAAACTTCT-3'	
MMP2	F: 5'-CCAGAAGGCGAACAGACTG-3'	NM_001320216.1
	R: 5'-TGGGCCGGAGACCTAAAGAG-3'	
MMP9	F: 5'-GCGTCGTGATCCCCACTTAC-3'	NM_013599.5
	R: 5'-CAGGCCGAATAGGAGCGTC-3'	
Notch1	F: 5'-TCAGTGGCCCTAATTGCCAG-3'	NM_008714.3
	R: 5'-ACCTCGCAGGTTTGACCTTG-3'	
Jag1	F: 5'-TCCTGTCCATGCAGAACGTG-3'	NM_013822.5
	R: 5'-CAAAGTGTAGGACCTCGGCCA-3'	
DLL4	F: 5'-TGGGACTCAGCAAGTGTGC-3'	NM_019454.3
	R: 5'-GTAGCTATTCTCCTGGTCCTTACA-3'	
HES1	F: 5'-CTACCCCAGCCAGTGTCAAC-3'	NM_008235.2
	R: 5'-ATGCCGGGAGCTATCTTTCT-3'	
HEY1	F: 5'-CTGAGCGTGAGTGGGATCAG-3'	NM_010423.2
	R: 5'-CGCCGAACTCAAGTTTCCAT-3'	
β-actin	F: 5'-GTACCACCATGTACCCAGGC-3′	NM_007393.5
	R: 5'-AACGCAGCTCAGTAACAGTCC-3'	

RT-qPCR, reverse transcription quantitative polymerase chain reaction; F, forward; R, reverse

then the protein concentration was measured and balanced among the different samples. After adding 5× loading buffer (CWBIO, Beijing, China), these mixtures were denatured at 100°C for 20 min. 10 μL of protein per lane were separated by 8%, 10%, or 12% sodium dodecyl sulfate-polyacrylamide gel and transferred to 0.45 mm PVDF membranes (Millipore, Shanghai, China). The membrane was blocked in 5% skim milk for 1 h at room temperature and then incubated with specific antibodies overnight at 4°C. The primary antibodies were: anti-Bmal1 (ab230822, Abcam, 1:2000), anti-VEGF (ab46154, Abcam, 1:2000), anti-VEGFR2 (26415-1-AP, Proteintech, 1:800), anti-MMP2 (10373-2-AP, Proteintech, 1:1000), anti-MMP9 (10375-2-AP, Proteintech, 1:1000), Angiogenin (18302-1-AP, Proteintech, 1:800), anti-Notch1 (10062-2-AP, Proteintech, 1:1500), anti-Hey1 (19929-1-AP, Proteintech, 1:2000), anti-Hes1 (A0925, Abclonal, 1:1500), anti-Jag1 (DF8269, Affinity, 1:1000), anti-DLL4 (A12943, Abclonal, 1:1500), and anti-β-actin (66009-1-Ig, Proteintech, 1:8000). The next day, the membrane was incubated with anti-rabbit horseradish peroxidase-conjugated secondary antibodies (E-AB-1003, Elabscience, China) for another 1.5 h at room temperature. The Efficient Chemiluminescence Kit (GEN-VIEW, Beijing, China) was used for signal detection and the results were recorded using the Bio-Rad ChemiDoc MP Gel Imaging System. The band density of specific proteins was quantified after normalization with the density of β-actin.

Statistical Analysis

Data analysis was performed using SPSS 24.0 statistical software (SPSS Inc., Chicago, IL, USA). Data are presented as the mean ± SD from at least three independent experiments. All data were subject to tests for normality. Data that did not have a normal distribution were analyzed *via* a non-parametric equivalent. Analysis of mNSS was implemented by the non-parametric Kruskal-Wallis test. When only two groups were compared, an unpaired two-tailed *t*-test was used. Multiple comparisons were evaluated by one-way or two-way ANOVA (with repeated measures when appropriate) followed by Tukey-Kramer tests or Bonferroni corrections, and $P < 0.05$ was considered statistically significant.

Results

Environmental Circadian Disruption Increases Stroke Severity and Impairs Angiogenesis-Related Factors in MCAO Rats

We used a precise schedule that lead to the temporary misalignment of central and peripheral clock genes during re-synchronization, and disruption within the central pacemaker itself [32, 42, 51] (Fig. 1A). As shown in Fig. 1B, the dorsal hair of rats with a normal circadian rhythm was white, thick, clean, and shiny, while the dorsal hair of ECD rats was greasy, gray-yellow, brittle, and partially shed. Representative brain images of TTC-stained areas showing infarct volumes in the three groups 24 h after cerebral ischemia-reperfusion injury (Fig. 1C). Infarct volume and 10-day neurological score were quantified separately, and as expected, the infarct volume and neurological score were significantly increased in the ECD group (Fig. 1D, E).

As noted above, angiogenesis occupies a large proportion of the collateral circulation and rehabilitation process after cerebral infarction. To further understand the damage mechanism of environmental circadian rhythm disturbance on cerebral infarction, we focused on the effect of ECD on angiogenesis after cerebral infarction. First, we found that the core biological clock gene Bmal1 showed a fluctuation that first decreased and then increased in the MCAO model. After 24 h of reperfusion, the expression of Bmal1 protein in the ischemic penumbra significantly decreased. On day 10, the expression of Bmal1 was significantly higher than at 24 h (Fig. 2A). HE staining showed the hippocampus, neurons, and glial cells in the control (Ctrl) group were arranged in an orderly manner and had a normal structure 24 h after surgery. MCAO hippocampal neurons were disordered, the cell membrane was damaged, the cell morphology was swollen, a large number of neurons were lost and dead, and some nuclei were dissolved, condensed, and pyknotic. Compared with the model group, neuronal necrosis, nuclear condensation of a pyknotic cell membrane, and structural destruction were all aggravated in the MCAO-ECD group (Fig. 2B). As shown in Fig. 2C, the protein levels of MMP-9 and VEGF, which are closely associated with angiogenesis, were upregulated in the MCAO group compared with the Ctrl group ($P < 0.05$) at 10 days after surgery, while these levels in the MCAO-ECD group were significantly lower than in the MCAO group ($P < 0.001$).

To further determine the relationship between ECD and angiogenesis, we imaged and quantified CD34 10 days after MCAO surgery. Compared with the Ctrl group, the microvessel density ($CD34^+$/Field) in the cortex and hippocampus was increased in the MCAO group, while that in the ECD intervention group was significantly lower than that in the model group ($P < 0.05$) (Fig. 2D). It is well known that inflammatory cells and cytokines affect the proliferation and migration of ECs [52, 53], so we next assessed the serum levels of the inflammatory cytokines IL-1β, IL-18, and TNF-α at the same time point. As shown in Fig. 2E, the serum levels of IL-1β ($P <0.001$), IL-18 ($P < 0.05$), and TNF-α ($P < 0.01$) in the MCAO group were higher than those in the Ctrl group, and the serum levels of IL-1β ($P < 0.05$) and TNF-α ($P < 0.01$) in the MCAO-ECD group were significantly higher than those in

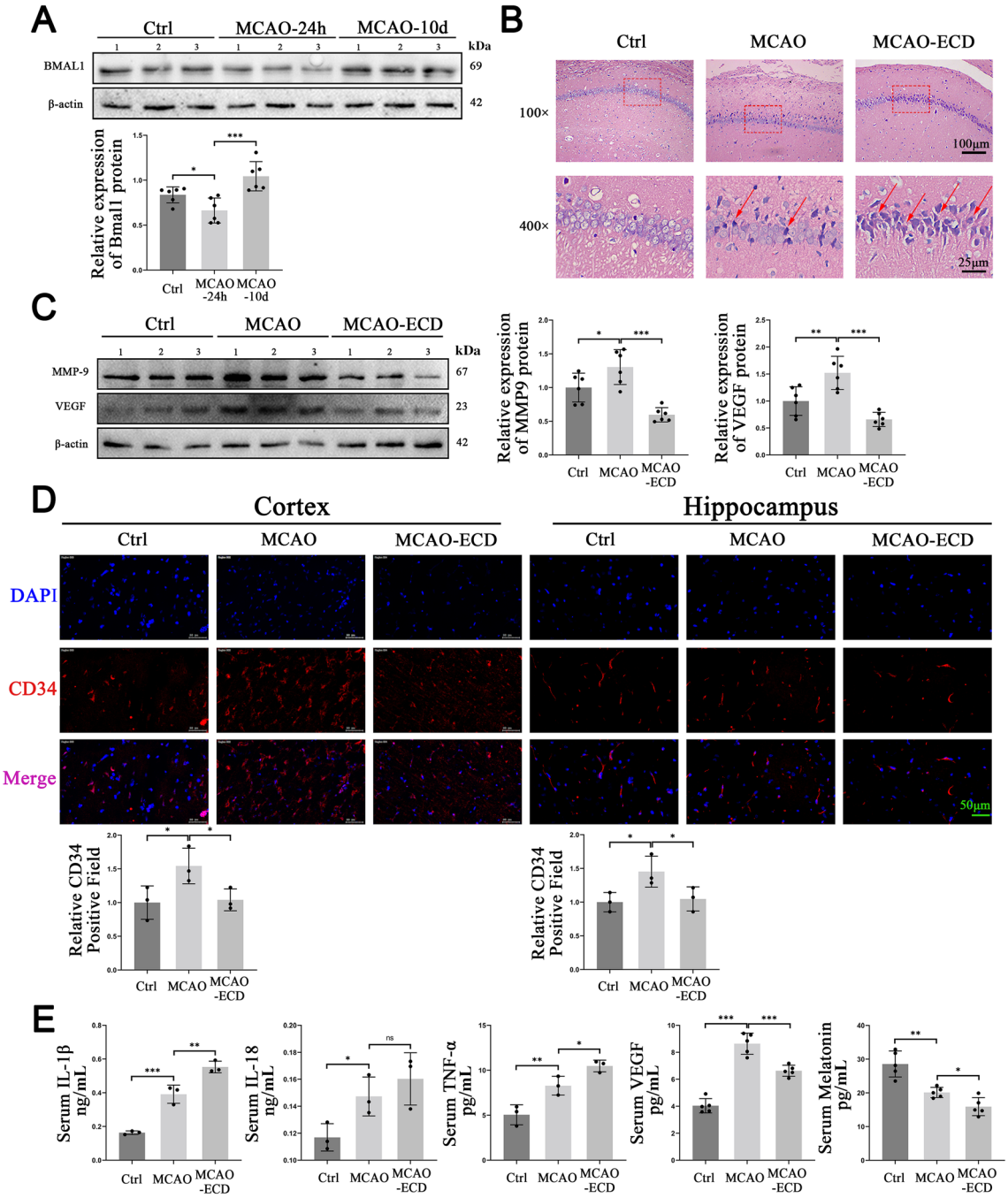

Fig. 2 ECD impairs angiogenesis-related factors in MCAO rats. **A** Western blots and statistics showing the changes of Bmal1 protein in brain tissue at different time points ($n = 6$). **B** HE staining showing the histopathological changes in the hippocampus of rats from each group [100× and 400× magnification; red indicates necrotic cells ($n = 3$)]. **C** Western blots and statistics showing the expression of MMP-2 and VEGF in the brains of each group ($n = 6$). **D** Representative immunofluorescence images and statistics of CD34 in the hippocampus and cortex 10 days after reperfusion. The Ctrl group was used as the control ($n = 3$). Scale bar, 50 μm. **E** Protein levels of IL-1β, IL-18, TNF-α, VEGF, and melatonin in rat serum were detected by ELISA (≥3). Data are presented as the mean ± SD. $^*P < 0.05$, $^{**}P < 0.01$, $^{***}P < 0.001$.

the MCAO group (Fig. 2E). More than this, the secretion of melatonin, which plays a critical role in the circadian rhythm in which the central and peripheral clocks operate synchronously [54], controls angiogenesis by regulating the expression of VEGF [55]. Significant reductions in serum VEGF ($P < 0.001$) and melatonin ($P < 0.05$) were also detected in our experiments (Fig. 2E).

Core Clock Gene Bmal1 Expression Is Upregulated in bEnd.3 Cells with OGD-evoked Injury

To investigate the changes in gene expression related to the circadian rhythm and angiogenesis in ECs after ischemic injury, we first established a bEnd.3-cell OGD/R model to mimic ischemia and reperfusion *in vitro*. We first treated bEnd.3 cells with dexamethasone for 2 h to induce cell cycle synchronization, followed by 6 h of OGD, and measured the changes of Notch1 intracellular domain (NICD), and Bmal1 protein at different time points. As shown in Fig. 3A–C, the protein level of Bmal1 and NICD expression were significantly upregulated at 12 h and 20 h, respectively, in the bEnd.3 cells with OGD-evoked injury ($P < 0.01$). More than this, we further explored changes in the angiogenesis-related gene expression patterns: Notch1 and VEGF mRNA were assessed by qPCR. As shown in Fig. 3D, the Notch1 mRNA level in the OGD group began to increase 4 h after OGD, and the rhythm of oscillation was strengthened. As for VEGF, apart from the 12th and 16th hours after OGD, the level of VEGF mRNA increased to varying degrees at each time point, and the amplitude of circadian oscillations was significantly enhanced (Fig. 3E).

Genome-Wide Characterization of Core Circadian Clock Bmal1 Transcriptional Binding Sites in bEnd.3 Cells

Bmal1 is known to be a pro-angiogenic transcription factor in ECs. However, the genomic binding pattern of Bmal1 in ECs remains unclear. To decipher the regulatory roles of Bmal1 in ECs, we applied ChIP-seq to determine the genome-wide target sites of Bmal1 in bEnd.3 cells. All three biological replicates showed high correlation scores >0.8 (Fig. 4A). The peaks over chromosomes had different values; among them, the most enriched peaks were on chromosome 1, and the peaks with the highest values were on chromosomes 5, 11, 14, and 15 (Fig. 4B). A total of 13,006 Ch-IP regions corresponding to 9,100 unique Ref-Seq genes were identified (Fig. 4C). Bmal1 binding sites at promoter transcription start sites accounted for 7.77% of the total reads (Fig. 4D). GO analysis of peak-related genes revealed that Bmal1 target genes were involved in various biological processes such as metabolism, protein modification, and translation initiation (Fig. 4E). KEGG analysis revealed that Bmal1 peak-related genes were significantly enriched in cell metabolism, including protein digestion and absorption, as well as the phospholipase and phosphatidylinositol pathways, and enriched in gap junction, axon guidance, and focal adhesion pathways, which promote intercellular communication and migration (Fig. 4F). We next used *de novo* motif

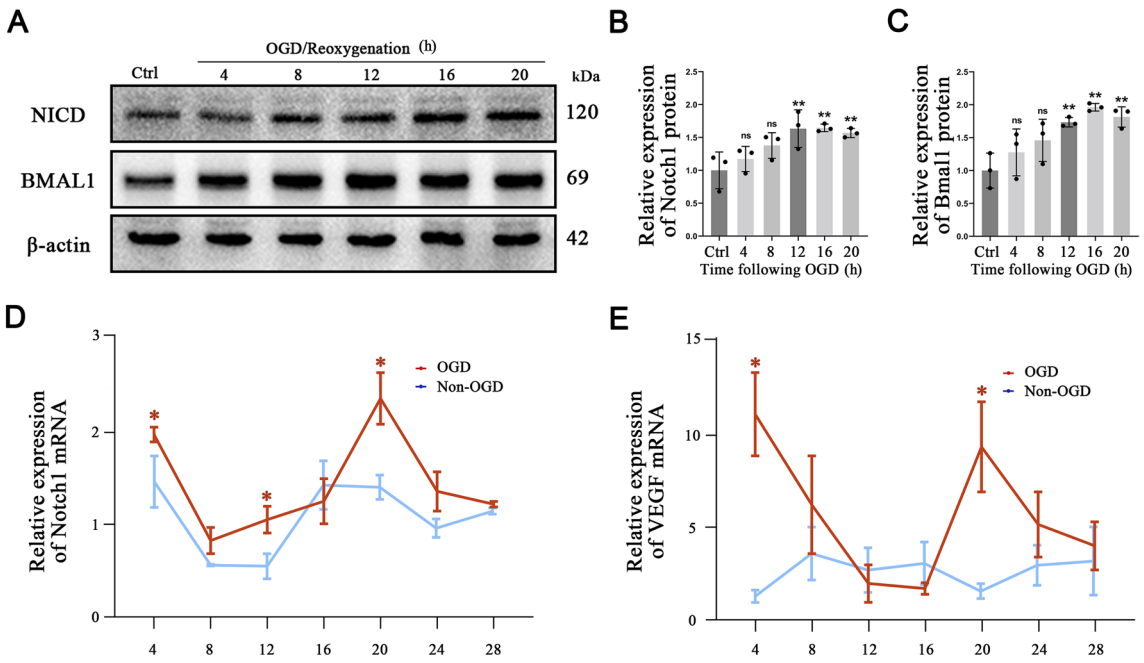

Fig. 3 The core clock gene Bmal1 expression is upregulated in OGD-evoked injury of bEnd.3 cells. **A–C** Western blots and analysis of the expression of NICD and VEGF protein in bEnd.3 cells at 4 h, 8 h, 12 h, 16 h, and 20 h after OGD treatment ($n = 3$). **D**, **E** Analysis of RT-qPCR showing the expression of Notch1 and VEGF mRNA in bEnd.3 cells at 4 h, 8 h, 12 h, 16 h, 20 h, 24 h, and 28 h after OGD exposure ($n = 3$). Data are presented as the mean ± SD. *P <0.05, **P <0.01, ***P <0.001.

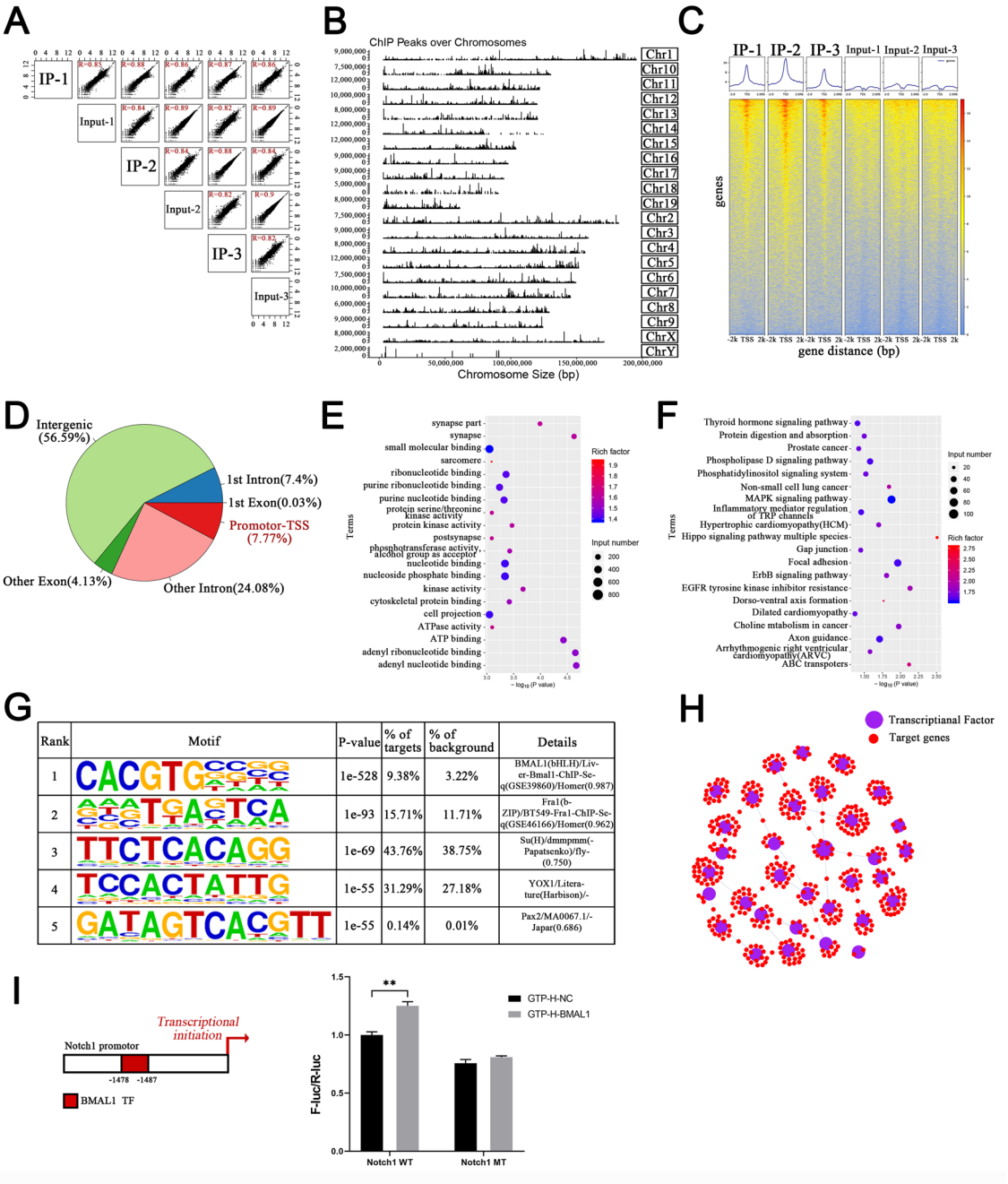

Fig. 4 Genome-wide characterization of core circadian clock Bmal1 transcriptional binding sites in bEnd.3 cells. **A** All three biological replicates show high correlation scores >0.8. **B** Using the primary antibody against Bmal1, ChIP-seq shows peaks on chromosomes (abscissa, chromosome length; right, chromosome number; left ordinate, peak value per chromosome). **C** The distribution of reads on both sides of the transcription start site. **D** Pie charts showing the ratio of Bmal1 binding sites relative to transcription units, including intergenic, exon 1, intron 1, TTS, promoter, other introns, and other exons. **E** GO enrichment of peak-related genes (top 20 terms). **F** KEGG enrichment map of metabolic pathways of peak-related genes (top 20 terms). **G** Five common motifs with the most significant differences among peaks. **H** Interaction network diagram between transcription factors and genes based on sequencing results (purple, transcription factor or transcription factor family; red, target genes on which transcription factors may act through motifs. **I** Dual luciferase activity assays using firefly luciferase reporter vectors; *Renilla* luciferase served as an internal control. The experiment was repeated three times. Data are presented as the mean ± SD. **P* <0.05; ***P* <0.01; ****P* <0.001.

discovery to investigate motifs shared between sequencing peaks and selected the five motifs with the most significant differences in presentation (Fig. 4G). Transcription factors can combine with these motifs, and the corresponding relationship between transcription factors and genes was drawn to map the interaction network (Fig. 4H).

VEGF and the Notch signaling pathway play a critical role in angiogenesis, and our *in vivo* research demonstrated that circadian rhythm disruption impaired the angiogenic activity, and confirmed the previous finding that overexpression of the core circadian clock Bmal1 significantly promotes the angiogenesis of various ECs. Similarly, we found that Bmal1 bound the enhancer region of Notch1 (position: chromosome2, 26463954–26464324), and the downstream gene Hes1 (position: chromosome16, 30066868–30067165; 30065082–30065373;30064015–30064496), and bound the promoter region of VEGF (position: chromosome17, 46030452–46030695). Dual-luciferase reporter assays also confirmed that Bmal1 bound directly to the enhancer region of Notch1 in bEnd.3 cells. The construction of the vector is shown in Fig. 4I. 293T cells were transfected with a luciferase expression vector containing the Notch1 promoter (−1478/−1487 -ggacacgcgc-) 5-flanking fragment. Luciferase reporter assays verified that Bmal1 overexpression increased the luciferase activity of Notch1-WT but had no inhibitory effect on that of Notch1-MUT (Fig. 4I).

Establishment of bEnd.3 Cells with Stable Overexpression and Silencing of Bmal1

To determine the exact effect of the core circadian clock Bmal1 on the angiogenesis process, three kinds of bEnd.3 cells were established: NC (control scrambled transfected cells), OE (Bmal1 gene overexpressing cells), and KD (Bmal1 gene knockdown cells). Bmal1-OE, Bmal1-KD, and negative control lentivirus were all transfected into bEnd.3 cells. After 72 h transfection, GFP was observed under the fluorescence microscope, and it was confirmed that the transfection efficiency was ~97% before proceeding to the next step (Fig. 5A). Then, the relative expression of Bmal1 mRNA and protein in transfected cells was verified by RT-qPCR and western blotting. The results of qPCR showed that, among the three designed siRNAs, the knockdown efficiency of Si2 reached >50%, and the expression level of overexpressed Bmal1 mRNA was >8-fold that of the NC group (Fig. 5B). Si2 significantly knocked down the protein expression of Bmal1, while the expression of Bmal1 in the OE group was significantly increased (Fig. 5C, D). Therefore, we chose si2-knockdown bEnd.3 cells for the follow-up experiments. Immunofluorescence showed that the expression of Bmal1 in the nucleus of the OE group was significantly increased, while that of the Si2 group was significantly decreased (Fig. 5E).

Bmal1 Is Required for Endothelial Angiogenesis *in Vitro*

We further tested the hypothesis that Bmal1, the core clock gene of the circadian rhythm, regulates the EC angiogenesis process according to the phenotype of circadian rhythm and angiogenesis shown in Figs. 1, 2, 3, 4. Since angiogenesis is a multistage process during which activated ECs sprout, migrate, proliferate, align, and form a tube, and anastomose, we applied tube formation assays, migration assays, and wound healing assays to reproduce these steps. The tube formation assays were used to test the angiogenic ability of bEnd.3 cells. In the body, ECs are surrounded by the basement membrane, a thin and highly specialized extracellular matrix. When ECs are inoculated on basement membrane-like surfaces such as Matrigel, they form capillary-like structures that reproduce angiogenesis *in vitro*. The transwell and cell scratch wound assays were used to test the migration ability of ECs. Due to the specific permeability of the polycarbonate membrane, the complete medium in the lower layer can affect the cells in the upper chamber, thereby reflecting the levels of cell chemotaxis and cell migration. Similarly, cell migration is also reflected in wound healing assays. A blank region is created on the fused monolayer of cells, and the cells at the edge migrate to the center after receiving a migration signal or sensing a gradient of pro-angiogenic regulatory factors, such as VEGF. The results revealed that Bmal1 depletion impaired the endothelial angiogenic ability, including tube formation, transwell, and wound healing (Fig. 6A–C).

To explore potential downstream effectors that might influence the Bmal1 loss-of-function phenotype, we investigated two known signaling pathways of ECs, namely, the VEGF-A and Notch-1-DLL4 signaling pathways, by RT-qPCR. Overexpression of Bmal1 increased the expression of angiogenesis-related factors, including VEGF ($P < 0.001$), MMP2 ($P < 0.001$), MMP9 ($P < 0.05$), and ANG ($P < 0.05$) (Fig. 6D). After knockdown of Bmal1, the expression of VEGF was significantly decreased ($P < 0.05$). The Notch1 signaling pathway plays a key role in angiogenesis and in vascular homeostasis, so the Notch receptor DLL4, ligand JAG1, and several Notch target genes including Hey1 and Hes1 were assessed by RT-qPCR. It is worth noting that we found that Notch1 ($P < 0.05$), DLL4 ($P < 0.01$), Hes1 ($P < 0.01$), and Hey1 ($P < 0.001$) were increased in the Bmal1-OE group compared with the NC group. However, the genes downstream from Notch1 remained unchanged in the Bmal1-KD bEnd.3 cell line (Fig. 6E). Overall, the stable Bmal1-knockdown cell line had a significantly reduced capacity for angiogenesis and downregulated angiogenic factors, and the results support the pivotal role of Bmal1 in bEnd.3 cells are involved in angiogenesis.

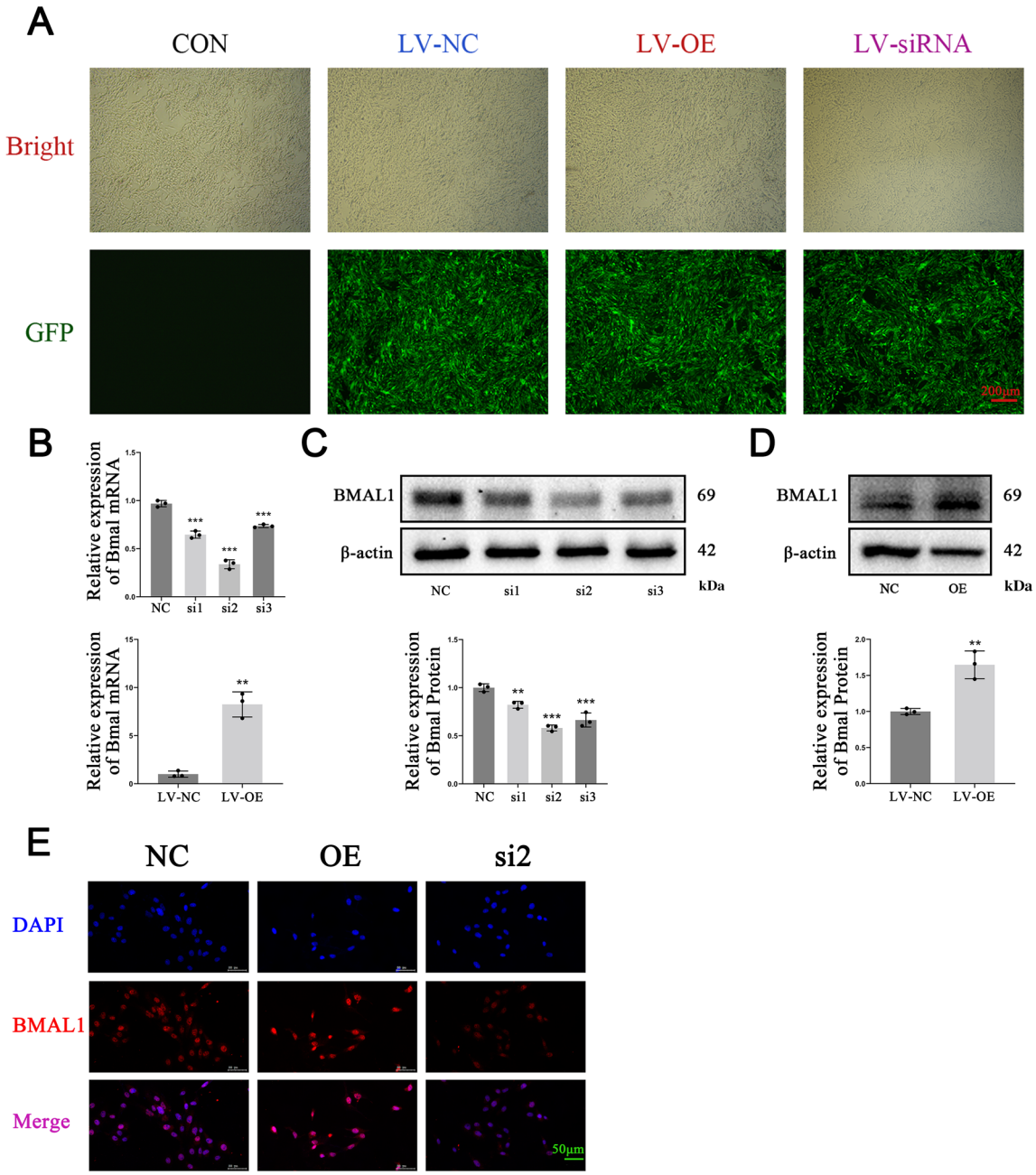

Fig. 5 Stable overexpression and silencing of Bmal1 in bEnd.3 cells. **A** Green fluorescent light density shows that the lentivirus plasmid is highly effectively integrated into the genome of bEnd.3 cells. **B** RT-qPCR analysis showing the mRNA of Bmal1 in the siRNA and OE groups. **C** Western blot results verify the knockdown efficiency of three siRNAs (Si1, Si2, and Si3) targeting different sites on Bmal1 in bEnd.3 cells and confirm that Si2 is the most effective siRNA for the knockdown of Bmal1 in bEnd.3 cells. **D** Western blots show that the Bmal1 protein is overexpressed in the OE group. **E** Representative immunofluorescence images of Bmal1 in bEnd.3 cells. Scale bar, 50 μm. Data are presented as the mean ± SD. $^{*}P < 0.05$, $^{**}P < 0.01$, $^{***}P < 0.001$.

Overexpression of Bmal1 Promotes the Proliferation and Accelerates Angiogenesis by OGD-injured bEnd.3 Cells by Regulating the VEGF/Notch1 Signaling Pathway

To evaluate the exact effect of Bmal1 on angiogenesis after ischemic stroke. We simulated the pathophysiological mechanism of ischemic stroke and constructed an *in vitro* OGD model of bEnd.3 cells, and applied a series of *in vitro* function measurements including CCK-8, scratch wound assays, migration assays, and tube formation assays.

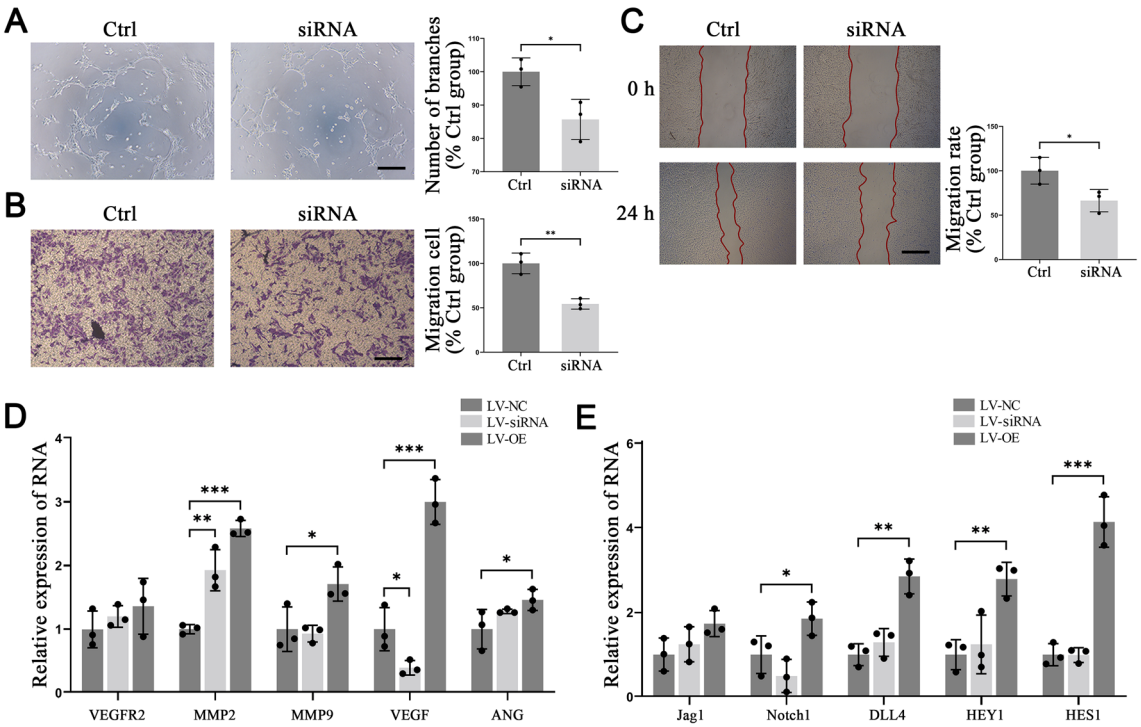

Fig. 6 Bmal1 is required for endothelial angiogenesis *in vitro*. **A** Representative microscopic images of tube formation in bEnd.3 cells transfected with control (Ctrl) and Bmal1 siRNA. Scale bar, 100 μm. **B** Phase-contrast microscopic images of bEnd.3 cells transfected with Bmal1 siRNA migrated and attached to the bottom membrane of a transwell. Scale bar, 100 μm. **C** Phase-contrast microscopic images of bEnd.3 cells transfected with Bmal1 siRNA at 0 and 24 h after scratching. Scale bar, 200 μm. **D** The expression of VEGF and angiogenesis-related gene mRNA as determined by RT-qPCR. **E** The expression of the Notch pathway and downstream gene mRNA as determined by RT-qPCR. Data are presented as the mean ± SD. **P* <0.05, ***P* <0.01, ****P* <0.001.

Cells in all groups were incubated in 96-well plates, and the cell proliferation at 24 h, 48 h, 72 h, and 96 h was assessed by CCK-8 assays (Fig. 7A). The results showed that there was no significant difference among the three groups at 24 h and 48 h ($P > 0.05$). The Bmal1-OE group showed a significant difference in cell proliferation rate at 72 h and 96 h compared with the NC group ($P < 0.05$). There was no significant difference in cell proliferation between the CON and NC groups ($P > 0.05$). Wound healing assays, tube formation assays, and transwell assays further confirmed the ability of Bmal1 to promote hypoxia-induced angiogenesis. We found that under normoxic conditions, the overexpression of Bmal1 significantly enhanced the migration of cells ($P < 0.01$), but in the tube formation and wound healing assays, no enhancement was found. The results of wound healing assays, tube formation assays, and transwell assays showed that under hypoxic conditions, the pro-angiogenic capacity of bEnd.3 cells were enhanced due to the massive secretion of VEGFA, VEGFR2, MMP2, MMP9, and ANG. And this enhancement was further strengthened in bEnd.3 cells overexpressing Bma11, regardless of the fact that the migration ability or the tube-forming ability were enhanced to varying degrees (Fig. 7B–D).

To further elucidate the protective mechanism of Bmal1 in bEnd.3 cells at the molecular level, we assessed angiogenesis and Notch1 signaling pathway-related proteins in bEnd.3 cells were exposed to OGD/R by immunofluorescence and western blots. Immunofluorescence assays showed that overexpression of Bmal1 further upregulated the protein expression of VEGF and Notch1 in both the cytoplasm and the nucleus during hypoxia-induced neovascularization (Fig. 7E–G). Moreover, we further assessed angiogenesis-related proteins by western blot, and the results suggested that overexpression of Bmal1 upregulated the protein levels of VEGF ($P < 0.05$) and MMP2 ($P < 0.01$) under normoxia, and the increased protein expression induced by hypoxia was further enhanced by Bmal1, including VEGF ($P < 0.001$), VEGFR2 ($P < 0.05$), MMP-2 ($P < 0.001$), and MMP-9 ($P < 0.05$) (Fig. 7H). Similarly, the protein levels of NICD ($P < 0.05$) and DLL4 ($P < 0.05$) were upregulated in bEnd3 cells overexpressing Bmal1. With the severity of OGD/R injury, the protein levels of the Notch-1 intracellular domain ($P < 0.001$), the related receptor Dll4 ($P < 0.01$), and the downstream proteins Hes1 ($P < 0.05$) and Hey1 ($P < 0.05$) were significantly increased. And overexpression of Bmal1

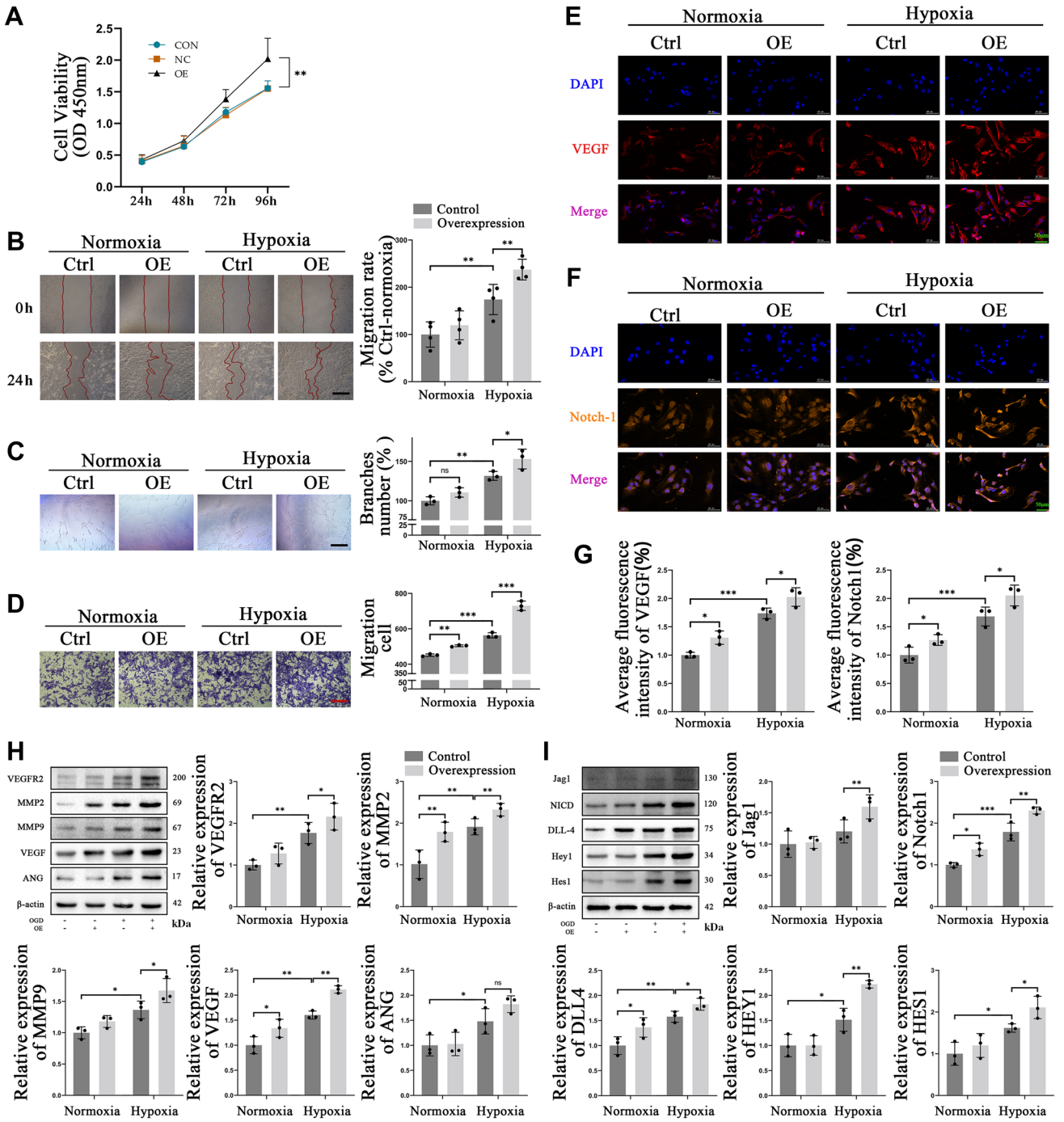

Fig. 7 Overexpression of Bmal1 promotes the proliferation and accelerates angiogenesis viability of OGDinjured bEnd.3 cells by regulating the VEGF/Notch1 signaling pathway. **A** CCK-8 assay shows that the proliferation of bEnd.3 cells significantly increases when Bmal1 is overexpressed. **B** Representative microscopic images of bEnd.3 cells at 0 and 24 h after scratching. Scale bar, 200 μm. **C** Representative microscopic images of tube formation in bEnd.3 cells. Scale bar, 100 μm. **D** Phase contrast microscopic images of bEnd.3 cells migrated and attached to the bottom membrane of a transwell. Scale bar, 100 μm. **E–G** Representative immunofluorescence images of VEGF (**E**), and Notch1 (**F**) in bEnd.3 cells. The bar chart shows the statistical results from three independent experiments (**G**). Scale bar, 50 μm. **H** The expression of VEGF and angiogenesis-related gene proteins as determined by western blot. **I** Western blots and analysis of the expression of the Notch pathway and downstream gene proteins. Data are presented as the mean ± SD. **P* <0.05, ***P* <0.01, ****P* <0.001.

further increased the expression of NICD ($P < 0.01$), the related receptors Jag1 ($P < 0.01$) and Dll4 ($P < 0.05$), and the downstream proteins Hes1 ($P < 0.05$) and Hey1 ($P < 0.01$) compared with the control group under hypoxic conditions (Fig. 7I).

Inhibition of the Notch1 Signaling Pathway Reverses the Effect of Overexpressed Bmal1 on Angiogenesis and Viability of OGD-injured bEnd.3 Cells

To further determine whether the Notch 1 signaling pathway is involved in the promotion of VEGF expression and regulation of angiogenesis by Bmal1, we used DAPT to intervene in bEnd.3 cells in subsequent studies, evaluating the role of Notch1 in this process by detecting the phenotype of angiogenesis and key proteins. DAPT is a potent γ-secretase inhibitor that inhibits the activation of Notch 1 signaling. Therefore, in phenotypic experiments, we added DAPT at the beginning of 24-h serum shock-induced cell cycle synchronization to inhibit activation of the Notch signaling pathway, and the intervention of DAPT continued until the end of the phenotype experiments. Under hypoxic conditions, DAPT significantly reduced the migration ($P < 0.01$) and tube-formation ($P < 0.01$) of EC (Fig. 8A, C). Consistent with the previous results, Baml1 significantly promoted the migration of ECs in the scratch wound ($P < 0.05$), transwell ($P < 0.001$), and tube formation assays ($P < 0.05$), but this promotion was partially reversed by DAPT (10 μmol/L). As shown in Fig. 8A–C, DAPT inhibited the pro-angiogenic effects of Bmal1, including migration and tubulogenesis, and we found a significant reversal in all three phenotypic experiments ($P < 0.001$). Western blot was further used to assess the expression of proteins closely related to the angiogenic process. First, we measured the protein level of NICD to verify the inhibitory effect of DAPT. The results showed that DAPT inhibited the activation process of NICD regardless of whether Bmal1 was overexpressed or not (Fig. 8D). Then the key molecules of angiogenesis were detected by western blot, as shown in Fig. 8D, and the expression of VEGF decreased after DAPT intervention, and the related proteins MMP-2 ($P < 0.01$), MMP-9 ($P < 0.01$), ANG ($P < 0.01$), and VEGFR2 ($P < 0.01$) were down-regulated to varying degrees. The results in this section revealed that the Notch1 signaling pathway plays a pivotal role in the process by which Baml1 regulates angiogenesis, and its potential mechanism may be a bridge between Bmal1 and VEGF.

Discussion

A growing body of literature suggests that the molecular, cellular, and physiological pathways of circadian rhythms are strongly associated with clinical outcomes in stroke [31]. Elucidating the complex and multifactorial influences of circadian rhythms may improve opportunities for clinical translation in stroke diagnosis and treatment. Changes in the light cycle can lead to ECD, causing a misalignment of the peripheral clock, negatively affecting the functioning of healthy organs, and accelerating the pathological processes of various diseases [32, 42, 56, 57]. A prior Cox proportional hazards model has shown that shift work is positively associated with the severity of ischemic stroke risk [58], suggesting that shift work leads to increased stroke risk and is an independent risk factor for ischemic stroke [59]. In animal models, phase-advancing light cycles increase the severity of stroke in MCAO/R rats [60].

Therefore, we mimicked the circadian disruption of inverted shift work *via* 6-h weekly advances in the 12:12 photoperiod; this promotes rapid phase changes in the suprachiasmatic nucleus (SCN), followed by changes in surrounding organs, and adjustment at different rates [61, 62]. Here, the ECD model was successfully established before the MCAO operation. In subsequent experiments, we assessed how advanced changes in the environmental LD cycle affect neural function and angiogenesis repair after ischemic injury. In an 8-week longitudinal study, we assessed neurological recovery at various time points after middle cerebral artery ischemic injury in rats, collecting brain and serum samples at 24 h and 10 days after infarction. The results showed that ECD increased the volume of cerebral infarction, as well as aggravating the degree of postoperative neurological injury, and impairing the ability to recover. The present study of the circadian rhythm was built on a growing body of evidence. Previous studies have shown that the circadian rhythm is a double-edged sword. On the one hand, the vascular circadian rhythm causes a stroke to occur in the morning with a hypercoagulable and hypofibrinolytic state; on the other hand, circadian rhythm disruption also seems to have an increased impact on stroke risk/severity [63]. In this study, the exact schedule of a 6-h phase advance was used to induce environmental circadian disruption; this results in temporary misalignment among central and peripheral oscillators, as well as misalignment within the central pacemaker itself during re-synchronization [32, 51]. Two points need to be clarified: one is whether the behavioral rhythm of running wheel exercise can modify the effect of ECD intervention, because running wheel monitoring is very important for the evaluation of circadian rhythms, and the other is that although ECD has been shown to aggravate stroke severity, the current study is superficial, whether ECD aggravates the outcome of ischemia by decreasing recovery (linked to angiogenesis) or by worsening the inflammation, aggravating blood-brain barrier destruction and other factors, therefore, the ECD effects on ECs, glial cells, and neuronal cells still need to be explored.

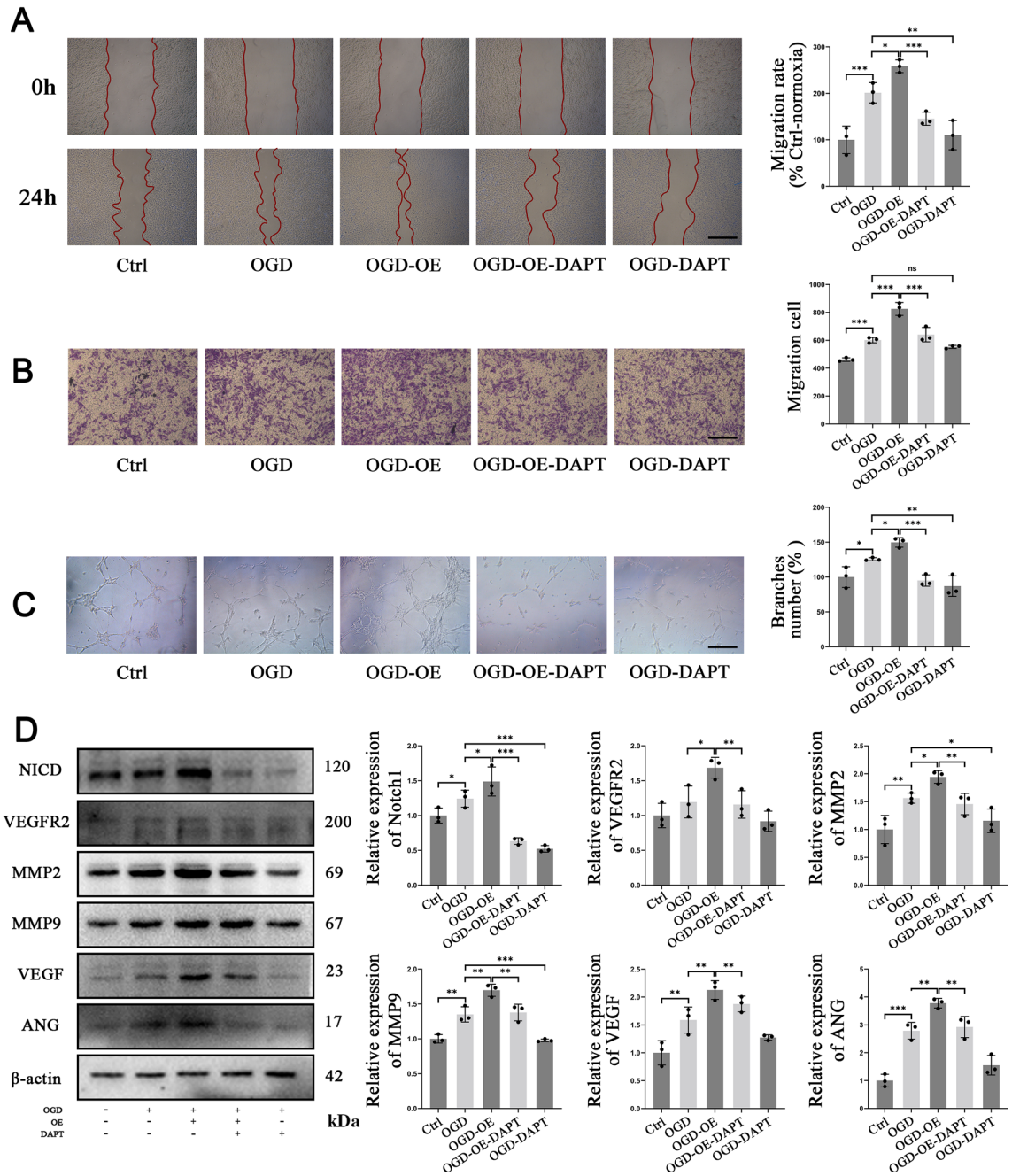

Fig. 8 Inhibiting the Notch1 signaling pathway reverses the effect of overexpressed Bmal1 on the angiogenesis viability of OGD-injured bEnd.3 cells. **A** Representative microscopic images of bEnd.3 cells were exposed to hypoxia and treated with DAPT at 0 and 24 h after scratching. Scale bar, 200 μm. **B** Phase-contrast microscopic images of bEnd.3 cells were exposed to hypoxia that migrated and attached to the bottom membrane of a transwell. Scale bar, 100 μm. **C** Representative microscopic images of tube formation in bEnd.3 cells exposed to hypoxia. Scale bar, 100 μm. **D** Western blots and analysis of the expression of VEGF, VEGFR2, MMP2, MMP9, and Ang. Data are presented as the mean ± SD. $^{*}P < 0.05$, $^{**}P < 0.01$, $^{***}P < 0.001$.

Angiogenesis is one of the key processes in the recovery mechanism of ischemic stroke, involving MMP-induced basement membrane degradation, VEGF-promoted cell proliferation, migration, and other functions [64]. Moreover, early zebrafish studies found that continuous light and the intervention of Bmal1 disrupt the circadian rhythm, thereby impairing developmental angiogenesis in zebrafish. It was further found that Bmal1 regulates the expression of VEGF and targets the VEGF gene promoter through the e-box region, which strictly regulates the development of

blood vessels [65]. Our rat research further found that ECD aggravated the pathological changes of MCAO, including the degree of cortical and hippocampal edema and neuronal damage in the infarcted hemisphere. More than this, ECD impaired angiogenesis, the number of CD34-positive cells in the infarcted hemisphere decreased significantly, and the expression of angiogenesis-related factors such as MMP-2 and VEGF decreased. Although angiogenesis requires a long time to build a functional vascular network infiltrating ischemic tissues, the transient expression of key angiogenic substances is still regulated by the circadian rhythm with diurnal differences [66]. It would be more convincing to measure the changes in the expression patterns of MMP2 and VEGF at different time points, rather than simply comparing the difference in expression between the same phase at day 10. In general, our data suggested that the transient dampening of rhythms during misalignment induced by light cycle changes may underlie neurological and vascular dysfunction in the brain, reducing resilience to the pathological damage of hypoxia in shift workers and ECD animal models.

Numerous studies have repeatedly shown that inflammation has a multistage and complex role in the development and pathogenesis of ischemic stroke [67]. On one hand, it is manifested as rhythmic changes in the number and movement of immune cells, and on the other hand, a large number of circadian clock genes have been confirmed to play an important role in the circadian function of immune cells. In the context of stroke, the immune system shows significant circadian rhythm changes, which affect the progress of recovery after stroke [68]. Although pro-inflammatory cytokines such as IL-1β and TNF-α promote angiogenesis, excessive pro-inflammatory cytokines can adversely affect the progression of angiogenesis [52, 53]. Therefore, we assessed the levels of IL-1 β, IL-18, and TNF-α in rat serum by ELISA, to explore the relationship between inflammation and angiogenesis. Interestingly, inflammatory factors were significantly higher in the ECD group than in the non-ECD group, and it was the excessive secretion of inflammatory factors that aggravated the neurological damage and impaired angiogenesis in MCAO rats. At the same time, as a key molecule regulating the circadian rhythm, melatonin can also affect angiogenesis in different scenarios by regulating the expression of VEGF and VEGF receptors [55]. The link between melatonin and angiogenesis is interesting; most previous experiments have focused on the anti-angiogenic potential of melatonin in tumor biology, however, recent studies indicate that melatonin is a clever hormone that can act according to the condition and location of the disease. Melatonin appears to inhibit or trigger angiogenesis through different signaling pathways, leading to different biological outcomes [69, 70]. In our study, we found that ECD decreased serum melatonin and VEGF levels, and the potential relationship between the two may be that melatonin downregulation leads to decreased VEGF secretion, which in turn impairs angiogenesis after cerebral infarction. Although we measured melatonin expression at the same circadian phase, however, as a key molecule regulating circadian rhythm, melatonin may largely be disturbed in the ECD animals, therefore, evaluation of melatonin levels over a complete 24 h cycle would be warranted in future studies.

Based on the above research *in vivo*, we found that the circadian rhythm regulates the process of angiogenesis after ischemic stroke and affects pathological processes to a certain extent. As the core transcriptional factor, Bmal1 regulates the circadian pattern of downstream gene expression [71]. Besides this, Bmal1 has been shown to promote angiogenesis in ischemia-injured human umbilical vein endothelial cells [72]. However, there is little evidence about the transcription function and epigenetic regulation of Bmal1. In subsequent experiments, we provided compelling evidence for the molecular mechanisms of how the circadian clock regulates repair angiogenesis following hypoxic injury. First, significant elevations of the core circadian clock Bmal1 were found in both MCAO rats and OGD-exposed bEnd.3 cells. Then, ChIP sequencing was used to identify the binding sites of Bmal1 on chromatin in bEnd.3 cells, to elucidate the genome-wide characterization of Bmal1, and to confirm the transcriptional regulation of Bmal1 and molecules associated with angiogenesis, including VEGF, Notch1, and Hey1. However, whether the transcriptional activity of Bmal1 differs in different tissues and cells, and whether it is related to the formation of transcriptional complexes with other proteins and genes, such as Clock-Bmal1 heterodimers, remains to be further investigated. We next showed that Bmal1 was required for the proliferation and angiogenesis of bEnd.3 cells under normoxia by using wound healing, transwell, and tube formation assays. And under the hypoxia, Bmal1 had a promoting effect on angiogenesis, by increasing the expression of VEGF and angiogenesis-related molecules.

The Notch pathway is a highly conserved intercellular signaling pathway that is critical for the development process of human tissues, organs, and phylogeny [73]. Receptors on the cell membrane can be activated and subjected to sequential proteolytic cleavage once the Notch ligand binds to it, then the Notch intracellular domain (NICD) is released and enters the nucleus to activate the transcription of the target genes. including Hey-1 and Hes-1, by complexing with the DNA-binding protein RBP-J and mediating the recruitment of histone acetylases and the transcriptional coactivator mastermind-like (MAML) [74]. Notch signaling limits vascular germination by limiting the formation of endothelial tip cells and maintaining arterial properties that depend on their relationship with VEGF [75]. In particular, the Notch signal is activated in ECs in response to ischemic stimulation and further participates in the formation of collateral networks in ischemic stroke [40, 76]. In our experiments,

we found that the NICD, Hes1, Hey1, and related receptors, such as Jag1 and DLL4 protein levels were upregulated in the OGD/R group, and further increased in the group overexpressing Bmal1. The results of ChIP-seq and dual-luciferase also confirmed that Bmal1 targets the regulation of Notch1 and Hes1 transcription in bEnd.3 cells. In previous studies, to determine the role of the Notch1 signaling pathway in cerebral infarction injury, a gamma-secretase inhibitor was often used to block the Notch1 pathway. Interestingly, DAPT has favorable pro-angiogenic effects *in vivo*, promoting post-stroke brain remodeling by elevating the cerebral blood flow [77], whereas DAPT abolishes the pro-angiogenic effects of human umbilical cord mesenchymal stem cells *in vitro* [78]. To verify whether Notch1 activation is involved in the pro-angiogenic effects of Bmal1 in bEnd.3 cells, DAPT was added to the co-culture medium before co-cultivation. The results showed that DAPT significantly abolished Notch1 activation in cells. More importantly, the addition of DAPT significantly reversed the pro-angiogenic effect of Bmal1, as evidenced by the inhibition of cell migration and tube formation, and reduced VEGF-A production.

Now that Bmal1 interacts with a variety of nucleic acids and proteins and participates in a variety of signaling pathways, however, how Bmal1 senses hypoxia signals to regulate the activation of VEGF and Notch1 is still unclear. Together, we have provided molecular insights into the mechanisms underlying the control of angiogenesis by Bmal1 under hypoxic conditions. A potential limitation of this study is that the sample size of animals under each detection index was a little small, but each measurement indicated the differences between the groups. We will use a larger sample in future studies, focusing on pathology and molecular biology.

In general, this is the first study to clarify the correlation between circadian rhythm and the occurrence and development of ischemic stroke, as well as the function and mechanism of action of Bmal1 in angiogenesis after ischemic stroke. Currently, several strategies have been proposed to correct clock disruption and desynchronization, to reduce the negative consequences if circadian rhythm impacts are unavoidable. These applications mainly include two aspects: environmental modifications and targeting-the-clock genes. Environmental modifications include high-intensity light, activity, and therapy during the day and night. Previous experiments have demonstrated that ambient light influences the occurrence and development of diseases. Mice exposed to low-dose light (5 lux) in the resting phase display a reduction of hippocampal VEGF and BDNF levels accompanied by depressive-like symptoms [79]. Thus, environmental light modifications may be a potential post-stroke therapy. More than this, circadian clocks regulate the molecular expression and functional state of angiogenesis to various extents, therefore another therapeutic strategy may be to change the phase of the circadian clock by manipulating the rhythmic phase of circadian clocks closer to the physiological state. As we described in this study, increasing the expression of Bmal1 after stroke promotes angiogenesis and the recovery of function after stroke. Thus, Bmal1 may also have therapeutic significance in promoting regeneration in ischemic vascular diseases.

Acknowledgements We would like to thank researcher Ping Li for excellent technical support. This work was supported by the National Natural Science Foundation for Young Scholars of China (82004346 and 82104766), the Natural Science Foundation of Hunan Province (2021JJ30521 and 2021JJ40424), the Open Fund for the First-class Discipline of Integrated Traditional Chinese and Western Medicine of Hunan University of Chinese Medicine (2020ZXYJH38 and 2020ZXYJH39), Natural Science Foundation of Changsha (kq2208202), and the University-level Fund Project of Hunan University of Chinese Medicine (2021XJJJ039).

Conflict of interest The authors declare that there are no conflicts of interest.

References

1. Johnson W, Onuma O, Owolabi M, Sachdev S. Stroke: A global response is needed. Bull World Health Organ 2016, 94: 634-634A.
2. Avan A, Hachinski V. Global, regional, and national trends of dementia incidence and risk factors, 1990–2019: A Global Burden of Disease study. Alzheimers Dement 2022, https://doi.org/10.1002/alz.12764.
3. Katan M, Luft A. Global burden of stroke. Semin Neurol 2018, 38: 208–211.
4. Tsao CW, Aday AW, Almarzooq ZI, Alonso A, Beaton AZ, Bittencourt MS. Heart disease and stroke statistics-2022 update: A report from the American heart association. Circulation 2022, 145: e153–e639.
5. Faizy TD, Mlynash M, Marks MP, Christensen S, Kabiri R, Kuraitis GM, *et al*. Intravenous tPA (tissue-type plasminogen activator) correlates with favorable venous outflow profiles in acute ischemic stroke. Stroke 2022, 53: 3145–3152.
6. Herpich F, Rincon F. Management of acute ischemic stroke. Crit Care Med 2020, 48: 1654–1663.
7. Peña-Martínez C, Durán-Laforet V, García-Culebras A, Cuartero MI, Moro MÁ, Lizasoain I. Neutrophil extracellular trap targeting protects against ischemic damage after fibrin-rich thrombotic stroke despite non-reperfusion. Front Immunol 2022, 13: 790002.
8. Hirano T. Evaluation of cerebral perfusion in patients undergoing intravenous recombinant tissue plasminogen activator thrombolysis. Neurol Med Chir (Tokyo) 2015, 55: 789–795.
9. Esposito E, Li W, Mandeville ET, Park JH, Şencan I, Guo S, *et al*. Potential circadian effects on translational failure for neuroprotection. Nature 2020, 582: 395–398.
10. Ruan L, Wang B, ZhuGe Q, Jin K. Coupling of neurogenesis and angiogenesis after ischemic stroke. Brain Res 2015, 1623: 166–173.
11. Jiang X, Suenaga J, Pu H, Wei Z, Smith AD, Hu X, *et al*. Post-stroke administration of omega-3 polyunsaturated fatty acids promotes neurovascular restoration after ischemic stroke in mice: Efficacy declines with aging. Neurobiol Dis 2019, 126: 62–75.
12. Uzdensky AB, Demyanenko S. Histone acetylation and deacetylation in ischemic stroke. Neural Regen Res 2021, 16: 1529–1530.

13. Bikfalvi A. History and conceptual developments in vascular biology and angiogenesis research: A personal view. Angiogenesis 2017, 20: 463–478.
14. Jin F, Zheng X, Yang Y, Yao G, Ye L, Doeppner TR, *et al*. Impairment of hypoxia-induced angiogenesis by LDL involves a HIF-centered signaling network linking inflammatory TNFα and angiogenic VEGF. Aging 2019, 11: 328–349.
15. Shweiki D, Itin A, Soffer D, Keshet E. Vascular endothelial growth factor induced by hypoxia may mediate hypoxia-initiated angiogenesis. Nature 1992, 359: 843–845.
16. Yang Y, Torbey MT. Angiogenesis and blood-brain barrier permeability in vascular remodeling after stroke. Curr Neuropharmacol 2020, 18: 1250–1265.
17. Krupinski J, Kaluza J, Kumar P, Kumar S, Wang JM. Role of angiogenesis in patients with cerebral ischemic stroke. Stroke 1994, 25: 1794–1798.
18. Wei L, Erinjeri JP, Rovainen CM, Woolsey TA. Collateral growth and angiogenesis around cortical stroke. Stroke 2001, 32: 2179–2184.
19. Chen J, Zhang ZG, Li Y, Wang L, Xu YX, Gautam SC, *et al*. Intravenous administration of human bone marrow stromal cells induces angiogenesis in the ischemic boundary zone after stroke in rats. Circ Res 2003, 92: 692–699.
20. Logan RW, McClung CA. Rhythms of life: Circadian disruption and brain disorders across the lifespan. Nat Rev Neurosci 2019, 20: 49–65.
21. Liu H, Qiu Z. Overexpression of MECP2 in the suprachiasmatic nucleus alters circadian rhythm and induces abnormal social behaviors. Neurosci Bull 2021, 37: 1713–1717.
22. Kollias GE, Stamatelopoulos KS, Papaioannou TG, Zakopoulos NA, Alevizaki M, Alexopoulos GP, *et al*. Diurnal variation of endothelial function and arterial stiffness in hypertension. J Hum Hypertens 2009, 23: 597–604.
23. Crnko S, Du Pré BC, Sluijter JPG, Van Laake LW. Circadian rhythms and the molecular clock in cardiovascular biology and disease. Nat Rev Cardiol 2019, 16: 437–447.
24. Lowrey PL, Takahashi JS. Genetics of circadian rhythms in mammalian model organisms. In: The Genetics of Circadian Rhythms. 1st ed. Amsterdam: Elsevier, 2011: 175–230.
25. Weber F, Zorn D, Rademacher C, Hung HC. Post-translational timing mechanisms of the *Drosophila* circadian clock. FEBS Lett 2011, 585: 1443–1449.
26. Preitner N, Damiola F, Luis-Lopez-Molina, Zakany J, Duboule D, Albrecht U, *et al*. The orphan nuclear receptor REV-ERBα controls circadian transcription within the positive limb of the mammalian circadian oscillator. Cell 2002, 110: 251–260.
27. Zhang Y, Fang B, Emmett MJ, Damle M, Sun Z, Feng D, *et al*. GENE REGULATION. Discrete functions of nuclear receptor Rev-erbα couple metabolism to the clock. Science 2015, 348: 1488–1492.
28. Mitsui S, Yamaguchi S, Matsuo T, Ishida Y, Okamura H. Antagonistic role of E4BP4 and PAR proteins in the circadian oscillatory mechanism. Genes Dev 2001, 15: 995–1006.
29. Cowell IG. E4BP4/NFIL3, a PAR-related bZIP factor with many roles. Bioessays 2002, 24: 1023–1029.
30. Gachon F, Fonjallaz P, Damiola F, Gos P, Kodama T, Zakany J, *et al*. The loss of circadian PAR bZip transcription factors results in epilepsy. Genes Dev 2004, 18: 1397–1412.
31. Lo EH, Albers GW, Dichgans M, Donnan G, Esposito E, Foster R, *et al*. Circadian biology and stroke. Stroke 2021, 52: 2180–2190.
32. Ramsey AM, Stowie A, Castanon-Cervantes O, Davidson AJ. Environmental circadian disruption increases stroke severity and dysregulates immune response. J Biol Rhythms 2020, 35: 368–376.
33. Koyanagi S, Kuramoto Y, Nakagawa H, Aramaki H, Ohdo S, Soeda S, *et al*. A molecular mechanism regulating circadian expression of vascular endothelial growth factor in tumor cells. Cancer Res 2003, 63: 7277–7283.
34. Sato F, Bhawal UK, Kawamoto T, Fujimoto K, Imaizumi T, Imanaka T, *et al*. Basic-helix-loop-helix (bHLH) transcription factor DEC2 negatively regulates vascular endothelial growth factor expression. Genes Cells 2008, 13: 131–144.
35. Jensen LD, Cao Y. Clock controls angiogenesis. Cell Cycle 2013, 12: 405–408.
36. Luo W, Garcia-Gonzalez I, Fernández-Chacón M, Casquero-Garcia V, Sanchez-Muñoz MS, Mühleder S, *et al*. Arterialization requires the timely suppression of cell growth. Nature 2021, 589: 437–441.
37. Lawson ND, Vogel AM, Weinstein BM. *sonic hedgehog* and *vascular endothelial growth factor* act upstream of the Notch pathway during arterial endothelial differentiation. Dev Cell 2002, 3: 127–136.
38. Liu ZJ, Shirakawa T, Li Y, Soma A, Oka M, Li Y, *et al*. Regulation of Notch1 and Dll4 by vascular endothelial growth factor in arterial endothelial cells: Implications for modulating arteriogenesis and angiogenesis. Mol Cell Biol 2003, 23: 14–25.
39. Al Haj Zen A, Oikawa A, Bazan-Peregrino M, Meloni M, Emanueli C, Madeddu P. Inhibition of delta-like-4-mediated signaling impairs reparative angiogenesis after ischemia. Circ Res 2010, 107: 283–293.
40. Cristofaro B, Shi Y, Faria M, Suchting S, Leroyer AS, Trindade A, *et al*. Dll4-Notch signaling determines the formation of native arterial collateral networks and arterial function in mouse ischemia models. Development 2013, 140: 1720–1729.
41. Castanon-Cervantes O, Wu M, Wu M, Paul K, Gamble KL, Johnson RL, *et al*. Dysregulation of inflammatory responses by chronic circadian disruption. J Immunol 2010, 185: 5796–5805.
42. Hill AM, Crislip GR, Stowie A, Ellis I, Ramsey A, Castanon-Cervantes O, *et al*. Environmental circadian disruption suppresses rhythms in kidney function and accelerates excretion of renal injury markers in urine of male hypertensive rats. Am J Physiol Renal Physiol 2021, 320: F224–F233.
43. Shen H, Pei H, Zhai L, Guan Q, Wang G. Salvianolic acid C improves cerebral ischemia reperfusion injury through suppressing microglial cell M1 polarization and promoting cerebral angiogenesis. Int Immunopharmacol 2022, 110: 109021.
44. Zhang L, Wei W, Ai X, Kilic E, Hermann DM, Venkataramani V, *et al*. Extracellular vesicles from hypoxia-preconditioned microglia promote angiogenesis and repress apoptosis in stroke mice *via* the TGF-β/Smad2/3 pathway. Cell Death Dis 2021, 12: 1068.
45. Yang D, Oike H, Furuse M, Yasuo S. Effect of regular and irregular stimulation cycles of dexamethasone on circadian clock in NIH3T3 cells. Chronobiol Int 2022, 39: 97–105.
46. Zong DD, Liu XM, Li JH, Ouyang RY, Long YJ, Chen P, *et al*. Resveratrol attenuates cigarette smoke induced endothelial apoptosis by activating Notch1 signaling mediated autophagy. Respir Res 2021, 22: 22.
47. Majumder S, Thieme K, Batchu SN, Alghamdi TA, Bowskill BB, Kabir MG, *et al*. Shifts in podocyte histone H3K27me3 regulate mouse and human glomerular disease. J Clin Invest 2018, 128: 483–499.
48. Lv S, Cai H, Xu Y, Dai J, Rong X, Zheng L. Thymosin-β 4 induces angiogenesis in critical limb ischemia mice *via* regulating Notch/NF-κB pathway. Int J Mol Med 2020, 46: 1347–1358.
49. Zhang Y, Liu T, Meyer CA, *et al*. Model-based analysis of ChIP-Seq (MACS). Genome Biol 2008, 9: R137.
50. Yu G, Wang LG, He QY. ChIPseeker: an R/Bioconductor package for ChIP peak annotation, comparison and visualization. Bioinformatics 2015, 31: 2382–2383.
51. Sellix MT, Evans JA, Leise TL, Castanon-Cervantes O, Hill DD, DeLisser P, *et al*. Aging differentially affects the re-entrainment

response of central and peripheral circadian oscillators. J Neurosci 2012, 32: 16193–16202.
52. Fahey E, Doyle SL. IL-1 family cytokine regulation of vascular permeability and angiogenesis. Front Immunol 2019, 10: 1426.
53. Zhang C, Zhu M, Wang W, Chen D, Chen S, Zheng H. TNF-α promotes tumor lymph angiogenesis in head and neck squamous cell carcinoma through regulation of ERK3. Transl Cancer Res 2019, 8: 2439–2448.
54. Cipolla-Neto J, Amaral FGD. Melatonin as a hormone: New physiological and clinical insights. Endocr Rev 2018, 39: 990–1028.
55. Ma Q, Reiter RJ, Chen Y. Role of melatonin in controlling angiogenesis under physiological and pathological conditions. Angiogenesis 2020, 23: 91–104.
56. West AC, Smith L, Ray DW, Loudon ASI, Brown TM, Bechtold DA. Misalignment with the external light environment drives metabolic and cardiac dysfunction. Nat Commun 2017, 8: 417.
57. Ding SL, Zhang TW, Zhang QC, Ding W, Li ZF, Han GJ, *et al*. Excessive mechanical strain accelerates intervertebral disc degeneration by disrupting intrinsic circadian rhythm. Exp Mol Med 2021, 53: 1911–1923.
58. Brown DL, Feskanich D, Sánchez BN, Rexrode KM, Schernhammer ES, Lisabeth LD. Rotating night shift work and the risk of ischemic stroke. Am J Epidemiol 2009, 169: 1370–1377.
59. Vyas MV, Garg AX, Iansavichus AV, Costella J, Donner A, Laugsand LE, *et al*. Shift work and vascular events: Systematic review and meta-analysis. BMJ 2012, 345: e4800.
60. Earnest DJ, Neuendorff N, Coffman J, Selvamani A, Sohrabji F. Sex differences in the impact of shift work schedules on pathological outcomes in an animal model of ischemic stroke. Endocrinology 2016, 157: 2836–2843.
61. Yamazaki S, Numano R, Abe M, Hida A, Takahashi R, Ueda M, *et al*. Resetting central and peripheral circadian oscillators in transgenic rats. Science 2000, 288: 682–685.
62. Davidson AJ, Yamazaki S, Arble DM, Menaker M, Block GD. Resetting of central and peripheral circadian oscillators in aged rats. Neurobiol Aging 2008, 29: 471–477.
63. Thosar SS, Butler MP, Shea SA. Role of the circadian system in cardiovascular disease. J Clin Invest 2018, 128: 2157–2167.
64. Tian J, Popal MS, Huang R, Zhang M, Zhao X, Zhang M, *et al*. Caveolin as a novel potential therapeutic target in cardiac and vascular diseases: A mini review. Aging Dis 2020, 11: 378–389.
65. Dahl Jensen L, Cao Z, Nakamura M, Yang Y, Bräutigam L, Andersson P, *et al*. Opposing effects of circadian clock genes *Bmal1* and *Period2* in regulation of VEGF-dependent angiogenesis in developing zebrafish. Cell Rep 2012, 2: 231–241.
66. Manoonkitiwongsa PS, Schultz RL, McCreery DB, Whitter EF, Lyden PD. Neuroprotection of ischemic brain by vascular endothelial growth factor is critically dependent on proper dosage and may be compromised by angiogenesis. J Cereb Blood Flow Metab 2004, 24: 693–702.
67. Zhu H, Zhang Y, Zhong Y, Ye Y, Hu X, Gu L, *et al*. Inflammation-mediated angiogenesis in ischemic stroke. Front Cell Neurosci 2021, 15: 652647.
68. Esposito E, Zhang F, Park JH, Mandeville ET, Li W, Cuartero MI, *et al*. Diurnal differences in immune response in brain, blood and spleen after focal cerebral ischemia in mice. Stroke 2022, 53: e507–e511.
69. Xu Y, Cui K, Li J, Tang X, Lin J, Lu X, *et al*. Melatonin attenuates choroidal neovascularization by regulating macrophage/microglia polarization *via* inhibition of RhoA/ROCK signaling pathway. J Pineal Res 2020, 69: e12660.
70. Rahbarghazi A, Siahkouhian M, Rahbarghazi R, Ahmadi M, Bolboli L, Keyhanmanesh R, *et al*. Role of melatonin in the angiogenesis potential; highlights on the cardiovascular disease. J Inflamm 2021, 18: 4.
71. Míková H, Kuchtiak V, Svobodová I, Spišská V, Pačesová D, Balík A, *et al*. Circadian regulation of GluA2 mRNA processing in the rat suprachiasmatic nucleus and other brain structures. Mol Neurobiol 2021, 58: 439–449.
72. Xu L, Liu Y, Cheng Q, Shen Y, Yuan Y, Jiang X, *et al*. Bmal1 downregulation worsens critical limb ischemia by promoting inflammation and impairing angiogenesis. Front Cardiovasc Med 2021, 8: 712903.
73. Liu J, Li Q, Zhang KS, Hu B, Niu X, Zhou SM, *et al*. Downregulation of the long non-coding RNA Meg3 promotes angiogenesis after ischemic brain injury by activating Notch signaling. Mol Neurobiol 2017, 54: 8179–8190.
74. Guruharsha KG, Kankel MW, Artavanis-Tsakonas S. The Notch signalling system: Recent insights into the complexity of a conserved pathway. Nat Rev Genet 2012, 13: 654–666.
75. Noguera-Troise I, Daly C, Papadopoulos NJ, Coetzee S, Boland P, Gale NW, *et al*. Blockade of Dll4 inhibits tumour growth by promoting non-productive angiogenesis. Nature 2006, 444: 1032–1037.
76. Takeshita K, Satoh M, Ii M, Silver M, Limbourg FP, Mukai Y, *et al*. Critical role of endothelial Notch1 signaling in postnatal angiogenesis. Circ Res 2007, 100: 70–78.
77. Tian JQ, Zheng JJ, Hao XZ, Yin LK, Zhang XX, Li CC, *et al*. Dynamic evaluation of Notch signaling-mediated angiogenesis in ischemic rats using magnetic resonance imaging. Behav Neurol 2018, 2018: 8351053.
78. Zhu J, Liu Q, Jiang Y, Wu L, Xu G, Liu X. Enhanced angiogenesis promoted by human umbilical mesenchymal stem cell transplantation in stroked mouse is Notch1 signaling associated. Neuroscience 2015, 290: 288–299.
79. Walker WH, Borniger JC, Gaudier-Diaz MM, Hecmarie Meléndez-Fernández O, Pascoe JL, Courtney DeVries A, *et al*. Acute exposure to low-level light at night is sufficient to induce neurological changes and depressive-like behavior. Mol Psychiatry 2020, 25: 1080–1093.